Paleoceanography and Paleoclimatology

RESEARCH ARTICLE
10.1029/2020PA004204

Key Points:

- Multiproxy study of Prydz Bay reveals warm conditions in East Antarctica before glacial advance at the Eocene-Oligocene Transition
- Biomarkers reveal abrupt cooling and drying at the Eocene-Oligocene Transition
- Marine productivity increased on the margins of Antarctica as icehouse conditions set in

Supporting Information:

Supporting Information may be found in the online version of this article.

Correspondence to:

E. J. Tibbett,
tibbett@usc.edu

Citation:

Tibbett, E. J., Scher, H. D., Warny, S., Tierney, J. E., Passchier, S., & Feakins, S. J. (2021). Late Eocene record of hydrology and temperature from Prydz Bay, East Antarctica. *Paleoceanography and Paleoclimatology*, *36*, e2020PA004204. https://doi.org/10.1029/2020PA004204

Received 20 DEC 2020
Accepted 6 APR 2021

Late Eocene Record of Hydrology and Temperature From Prydz Bay, East Antarctica

Emily J. Tibbett[1], Howie D. Scher[2], Sophie Warny[3], Jessica E. Tierney[4], Sandra Passchier[5], and Sarah J. Feakins[1]

[1]Department of Earth Science, University of Southern California, Los Angeles, CA, USA, [2]Department of Earth and Ocean Sciences, University of South Carolina, Columbia, SC, USA, [3]Department of Geology and Geophysics, Louisiana State University, Baton Rouge, LA, USA, [4]Department of Geosciences, University of Arizona, Tucson, AZ, USA, [5]Department of Earth and Environmental Studies, Montclair State University, Montclair, NJ, USA

Abstract The Eocene-Oligocene transition (EOT) marks the onset of Antarctic glaciation at 33.7 Ma. Although the benthic oxygen isotope record defines the major continental ice sheet expansion, recent sedimentary and geochemical evidence suggests the presence of earlier ephemeral ice sheets. Sediment cores from Ocean Drilling Program Legs 119 and 188 in Prydz Bay provide an archive of conditions in a major drainage system of East Antarctica. We study biomarker and microfossil evidence to discern how the vegetation and climate shifted between 36 and 33 Ma. Pollen was dominated by reworked Permian Glossopterid gymnosperms; however, penecontemporaneous Eocene pollen assemblages indicate that some vegetation survived the glacial advances. At the EOT, brGDGT soil biomarkers indicate abrupt cooling from 13°C to 8°C and soil pH increases from 6.0 to 6.7, suggesting drying which is further supported by plant wax hydrogen and carbon isotopic shifts of 20‰ and 1.1‰, respectively, and evidence for drying from weathering proxies. Although the terrestrial soil biomarker influx mostly precludes the use of TEX_{86}, we find sea surface temperatures of 12°C in the late Eocene cooling to 8°C at the EOT. Marine productivity undergoes a sustained increase after the glacial advance, likely promoted by enhanced ocean circulation. Between the two glacial surge events of the Priabonian Oxygen Maximum at 37.3 Ma and the EOT at 33.7 Ma, we observe warming of 2–5°C at 35.7 and 34.7 Ma, with increase in penecontemporaneous pollen and enhanced marine productivity, capturing the last flickers of Antarctic warmth.

Plain Language Summary Antarctica, once covered in forests and diverse vegetation, became almost fully ice covered around 33.7 million years ago. However, there are few records of conditions before the ice advanced. Seafloor mud, off the Antarctic coast, holds clues to conditions on land, before ice expanded to cover the continent. Pollen grains indicate what species of plants were growing at the time. We use molecular evidence from plant leaves and soils to reconstruct rainfall. Other lines of evidence include temperature estimates from soil and seawater microbes. Together these lines of evidence reveal warm periods in the Late Eocene and a cooling and drying climate with enhanced erosion as ice advanced. This helps to illuminate how conditions changed on land before Antarctica became fully ice covered, and can help check climate model simulations. This study provides a better understanding of how the Earth shifts between warm and cold climate states.

1. Introduction

The Eocene-Oligocene transition (EOT) is a period of ~790 kyr (34.2–33.5 Ma) that encompasses the chronostratigraphic Eocene-Oligocene Boundary at 33.9 Ma (Coxall & Pearson, 2007; Gradstein & Ogg, 2012; Hutchinson et al., 2021). The EOT marks the shift from the greenhouse conditions of the Eocene to the icehouse conditions of the Oligocene. A two-step increase in benthic foraminiferal oxygen isotopes ($\delta^{18}O_{benthic}$) of ~1.5‰ (Coxall et al., 2005; Zachos et al., 2001), the latter and larger of which is now referred to as the Earliest Oligocene Isotope Step (EOIS; Hutchinson et al., 2021) reflects a 2.5°C cooling of bottom waters and growth of a continent-wide ice sheet on Antarctica (Bohaty et al., 2012; Lear et al., 2008). The cooling of bottom waters (Lear et al., 2008) leaves 0.6‰ of the $\delta^{18}O_{benthic}$ shift as an increase in seawater ($\delta^{18}O_{seawater}$), suggesting an ice sheet 60%–130% of modern East Antarctic Ice Sheet at 33.7 Ma (Bohaty et al., 2012). Clumped isotopes applied to microfossils from Ocean Drilling Program (ODP) Site 689 determined a similar

increase in $\delta^{18}O_{seawater}$ of 0.75‰, suggesting an ice sheet 110%–120% of modern (Petersen & Schrag, 2015). Evidence for the growth of ice sheets comes from ice-rafted debris (Zachos et al., 1992), the development of ice-proximal fjord sediments in the Prince Charles Mountains (McKelvey et al., 2001), and a negative excursion in seawater εNd ($^{143}Nd/^{144}Nd$ sample ratio relative to the chondritic uniform reservoir in parts per 10,000) in the Southern Ocean corresponding to a surge of glacial erosion (Scher et al., 2011, 2014).

One of the leading theories for the glaciation of Antarctica at the EOT is that a decline in atmospheric pCO_2 led to ice initiation and expansion on the southern continent (DeConto et al., 2008; Hutchinson et al., 2021). Alkenone $\delta^{13}C$ evidence suggests a decline in atmospheric pCO_2 from 1,200–1,000 ppmv pre-EOT to 700–600 ppmv post-EOT (Pagani et al., 2011; Zhang et al., 2013). Independent estimates of post-EOT atmospheric pCO_2 range from 930 to 550 ppmv, inferred from the boron isotopic composition ($\delta^{11}B$) of planktic foraminifera (Anagnostou et al., 2016; Pearson et al., 2009). Climate modeling supports the hypothesis that pCO_2 drove cooling of the southern continent and ocean, which would have intensified Antarctic bottom water formation explaining the paleoceanographic changes seen further afield. The earlier hypothesis that suggested the opening of the Drake Passage and Tasman Gateway led to the thermal isolation of Antarctica (Kennett, 1977) is no longer considered viable, since the timing of gateway opening does not support such a linkage (Hill et al., 2013; Scher et al., 2015). Instead, εNd reconstructions from the Kerguelen Plateau offshore from Prydz Bay, reveal no change in the Southern Ocean circulation across the EOT (Wright et al., 2018), and instead find intensification of circulation over the Kerguelen Plateau as well as between Tasmania and Antarctica over 2 million years before the EOT from 35.7 Ma (Houben et al., 2019; Wright et al., 2018).

On Antarctica, archives of the latest Eocene are limited by modern glacial ice cover, with accessible outcrops only on the very northern limits at 64°S on Cockburn Island (Askin et al., 1991), on Seymour Island (Ivany et al., 2011), King George Island (Warny et al., 2019), or on exposed land in the Transantarctic Mountains marking the boundary between East and West Antarctica (Ashworth et al., 2007). Other records of conditions before glaciation come from drilling expeditions around the continental margin such as the SHALDRIL expedition off the tip of the Antarctic Peninsula (63°S) that captured a short window of time before the EOT (Anderson et al., 2011; Warny & Askin, 2011). Those sediments yielded pollen and plant wax, with carbon isotopic analyses ($\delta^{13}C$) on the pollen yielding evidence for cooling and drying (Feakins et al., 2014; Griener et al., 2015). Hydrogen isotopic (δD) analyses on the plant waxes yielded precipitation isotopic estimates similar to modern, that is, low sensitivity to the huge changes between ephemeral glaciation and the glaciated continent today (Feakins et al., 2014). Larger environmental changes are expected in the continental interior, and the largest drainage basin of East Antarctica is a strong candidate for delivering interior sediments to the margins.

Between the Kerguelen Plateau and the East Antarctic margin lies Prydz Bay (Figure 1), drilled by ODP Legs 119 and 188 (Barron et al., 1991; O'Brien et al., 2001), ideally placed to assess the exported signals of conditions on land in the glacio-fluvial catchment from the Gamburtsev mountains, today the largest outflow from the EAIS (Shepherd et al., 2018). Ice sheets expanded at the EOT, and had likely already initiated at the Gamburtsev Mountain peaks (in the southern corner of Figure 1b) in the latest Eocene (Rose et al., 2013), expanding toward the sea, via the Lambert Graben (Figures 1b and S1), during the EOT ice expansion. During the late Eocene, weathering proxies from the Prydz Bay sediments suggest mean annual air temperatures (MAATs) were >10°C at 35 Ma and suggest a gradual cooling to 8°C across 2 million years, without any abrupt cooling inflections detected although with two warm spikes during the late Eocene including at 35.7 Ma (Passchier et al., 2013, 2017). Pollen analysis from 35.7 Ma indicates a late Eocene *Nothofagus*-gymnosperm community with species tolerances suggesting MAAT below 12°C and precipitation around 1,200–2,500 mm/year (Macphail & Truswell, 2004; Truswell & Macphail, 2009). We return to these legacy cores with new and classic biomarker and microfossil techniques to reconstruct paleoenvironments in the 3 million years of the latest Eocene and across the EOT.

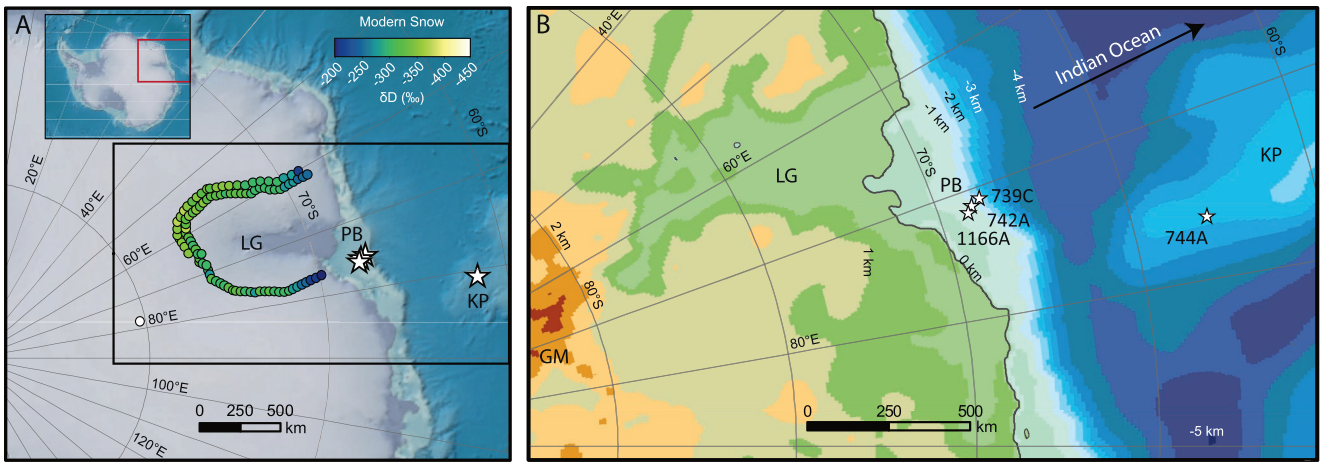

Figure 1. Map of Prydz Bay study location. (a) Modern conditions on the East Antarctic Ice Sheet (NOAA National Centers for Environmental Information); inset map shows whole Antarctic continent, red box for region shown in (a). Plotting δD values of modern snow samples from the Lambert Glacier (Delmotte, 1997) and Dome A (~80°S, ~77°E; Masson-Delmotte et al., 2008) with D-depletion inland (circle symbols, color legend). Black box denotes region expanded in (b). (b) Reconstructed topography and maximum bathymetry at 34 Ma (Hochmuth, Paxman, et al., 2020) showing the Gamburtsev Mountains (GM) Lambert Graben (LG), Prydz Bay (PB), and Kerguelen Plateau (KP), black contour denotes the EOT coastline. White stars indicate the Prydz Bay continental shelf locations of ODP Sites 739C (67°16.57′S, 75°04.91′E, 412 m), 742A (67°32.98′S, 75°24.27′E, 416 m), 1166A (67°41.77′S, 74°47.22′E, 475 m) and Kerguelen Plateau Site 744A (61°34.66′S, 80°35.46′E, 2307 m), studied here. Arrow indicates direction of the Indian Ocean.

2. Materials and Methods

2.1. Site Selection

For this study, we selected ODP Leg 119 Sites 739, 742 and Leg 188 Site 1166 from Prydz Bay located in the Indian Ocean sector of the Southern Ocean offshore of the modern coastline of East Antarctica (Figure 1a). Sites 739, 742, and 1166 are geographically adjacent, on the continental shelf at water depths of 412, 416, and 475 m, respectively, and together form a chronostratigraphy that has been previously used to describe sedimentology and track weathering proxies across 36–33 Ma, including 34.2–33.5 Ma encompassing the EOT (Passchier et al., 2013, 2017). The continental margin is at the outflow of the Lambert Glacier Amery Ice Shelf System that originates from the Gamburtsev Mountains and flows through the Lambert Graben (O'Brien et al., 2001) draining much of what is today covered by the EAIS (Figure 1a). The Lambert Graben is part of the Indian Mahanadi Rift System that formed during the separation of India and Antarctica at roughly 130 Ma (Harrowfield et al., 2005).

Paleotopographic reconstructions indicate coastline transgressions and regressions around the Lambert Graben varies with isostatic and eustatic changes (Hochmuth, Gohl, et al., 2020; Paxman et al., 2019) (Figure 1b; see also 3D map Figure S1). The latter aligns with fluvial/deltaic sandstones in the oldest sediments within Hole 1166A (O'Brien et al., 2001). Hole 742A, slightly inland and younger, consists primarily of mudstone and sandstone in the late Eocene suggesting a proximal glaciolacustrine or protected marine environment (Erohina et al., 2004). Approaching and spanning the EOT, in Hole 739C, the lithology shifts to diamictite with mud intraclasts (Erohina et al., 2004; Passchier et al., 2017) suggesting input from glaciers and proximity to grounded ice. Samples for the biomarker and pollen analyses here were selected to complement prior work on major element geochemistry. The age model is based on previous work on biostratigraphy, magnetostratigraphy, and seismostratigraphy with ages updated to GTS 2012 geologic timescale (Passchier et al., 2017 and references within). The 61 samples span from 35.8 to 32.9 Ma at ~50 ka resolution.

In addition, the Kerguelen Plateau, 700-km offshore from the Prydz Bay sites, was assessed for biomarker presence. ODP Site 744 (2,307-m water depth) is located on the Southern Kerguelen Plateau, and is dominated by nannofossil ooze. We selected 10 samples from Hole 744A across the same 32.9–35.8 Ma time span to sample a more distal location that had yielded a strong signal of glacial advance based on the εNd transported by ocean currents (Scher et al., 2014). The goal was to assess the presence of wind-blown terrigenous plant waxes and to seek ocean temperature reconstructions using the isoGDGT-based TEX_{86} biomarker

approach in the open Southern Ocean. However, no detectable biomarkers were recovered from 20 g samples; thus, no record of conditions at this site was possible.

2.2. Age Model

We used a previously reported paleomagnetic and biostratigraphic age model from Passchier et al. (2017) on GTS 2012 (Gradstein & Ogg, 2012). Age control tie points occur every 100–200 m in the ~400 m sedimentary sequence compiled from three sites. The age control includes paleomagnetic tie points constrained by biostratigraphy in the mudstones at the top of Hole 1166A. 1166A includes very high sedimentation rates (50.9 cm/kyr) with 100 m deposited between two age control points separated by 0.2 Ma at 35.9 and 35.7 Ma; between which, the ages for individual samples are constrained to within ~200 ka. The bottom age of 35.7 Ma is constrained by a stratigraphic tie at 304.29 mbsf in Hole 742A to 136.32 mbsf in Hole 1166A, where the 15r chron reversal is found. Although a fossil biostratigraphic datum (LO *Vozzhenikovia* sp. and *Deflandrea* sp. A) was described in 742A, the higher stratigraphic last appearance in 739C (shown) would be closer to the extinction in the water column, but as the duration of chron 13r to which the FO is tied is >1 Myr, it does not further constrain the age model. Across 35.7 to 33.6 Ma, sedimentation rates average 14.8 cm/kyr; lithology indicates likely changes in sedimentation rate, but they cannot be constrained due to the lack of additional age constraints. Biostratigraphic constraints are sparse and the first or last appearance of species have long spans (>1 Ma), as a result, uncertainties may be as large as 1 Ma. The long duration of chron 13r and the lack of additional biostratigraphic age control between 35.7 and 33.7 Ma, prohibit high-resolution temporal correspondence with regional and global records across the entire 2-Myr interval. However, the 35.7 Ma warming near the beginning of this record and the EOT cooling at 33.7 Ma are constrained to within ~200 ka.

2.3. Palynology

For palynology, samples were processed for terrestrial palynomorphs at Global Geolab Limited (Alberta, Canada). Dry sediment was weighed and spiked with a known quantity of *Lycopodium* spores to allow for evaluation of palynomorph concentrations. Dry sediment was successively treated with hydrochloric acid, hydrofluoric acid, and heavy liquid separation (Brown et al., 2008). Samples were sieved between a 10 and 250 μm fraction, and the remaining residue was mounted on microscope slides using glycerin jelly. Palynological analysis was conducted on a subset of 39 samples in the Louisiana State University's Center for Excellence in Palynology (CENEX) lab. Recovery was excellent and 300 palynomorphs were tabulated for each sample using an Olympus BX41 microscope. Concentrations were calculated as:

$$C = \left(P_C \times L_t \times T\right) / \left(L_C \times W\right) \quad (1)$$

where C = concentration (counts per gram of dried sediment, gdw^{-1}), P_c = the number of palynomorphs counted, L_t = the number of *Lycopodium* spores per tablet, T = the total number of *Lycopodium* tablets added per sample, L_c = the number of *Lycopodium* spores counted, W = the weight of dried sediment. Palynomorphs were identified to the lowest taxonomic level possible. Data reported provides counts of spores, southern beech tree (i.e., *Nothofagus*), other angiosperms, gymnosperms, and reworked pollen grains (likely of Permian age but potentially as young as Jurassic age), each reported as a % of all terrestrial spores and pollen. Where present in unusual quantity, charcoal or coal fragments were noted.

2.4. Extraction of Lipids and Quantification of *n*-Alkanes and *n*-Alkanoic Acids

Prydz Bay sediment samples ranging from 10 to 50 g were ground with a mortar and pestle then weighed. Leaf waxes were extracted using a DIONEX Accelerated Solvent Extractor using a 9:1 (*v/v*) dichloromethane (DCM) to methanol solution at 100°C and 1,500 psi for two 15-min cycles. The total lipid extract was separated into a neutral and acid fraction using an NH_2 Sepra column eluted with a 2:1 (*v/v*) ratio of DCM:isopropanol (neutral fraction) and 4% formic acid in diethyl ether (acid fraction). The neutral fraction was separated over silica gel eluting alkanes with hexanes and then the polar fraction was eluting first with DCM and then with methanol. The acid fraction was methylated overnight with methanol of a known isotopic concentration and hydrochloric acid (95:5) and dried using an anhydrous sodium sulfate column

yielding the fatty acid methyl esters (FAMEs). The FAMEs were purified using a silica gel column eluting first with hexane, and then collecting the FAMEs with DCM. An additional silver nitrate column was used to remove unsaturated compounds from the FAMEs fraction that would coelute and interfere with isotopic determinations. Alkane and FAMEs were identified by gas chromatography-mass spectrometry (GC-MS). We also screened the alkanes fraction for the presence of hopanes, biomarkers that derive from membrane lipids in bacteria and undergo isomerization with increasing thermal maturity, using their diagnostic mass fragments and published spectra (Inglis et al., 2018; Sessions et al., 2013; Uemura & Ishiwatari, 1995), and noted where those samples included an uncharacterized complex mixture. The samples were quantified by GC-FID (gas chromatography-flame ionization detector) relative to in house standards of alkanes and FAMEs of known concentration. We report the concentration of C_{16}–C_{30} *n*-alkanoic acids and C_{17}–C_{29} *n*-alkanes and calculate the summed C_{17}–C_{29} alkanes and summed C_{16} to C_{30} FAMEs in ng/gdw. We also calculate the average chain length (ACL) and carbon preference index (CPI) using the following formulae:

$$\text{ACL:} \; {\Sigma\left(n * \left[C_n\right]\right)} \Big/ {\Sigma\left[C_n\right]} \tag{2}$$

$$\text{CPI}: \; {2\Sigma C_n} \Big/ {\left(\Sigma C_{n+1} + \Sigma C_{n-1}\right)} \tag{3}$$

where *n* is 24–30 for *n*-alkanoic acids and 23–29 for *n*-alkanes.

2.5. Compound Specific Isotopic Analyses: $\delta^{13}C$ and δD

Compound specific isotope analysis was performed using a gas chromatography-isotopic ratio mass spectrometer (GC-IRMS) using a Thermo Scientific Trace gas chromatograph connected to a Delta V Plus mass spectrometer via an Isolink combustion furnace at 1,000°C for $\delta^{13}C$ and a pyrolysis furnace at 1,400°C for δD. The peak amplitude was 1–7 V. $\delta^{13}C$ linearity was recorded each day and had an average standard deviation of 0.042‰. H_3 factor was recorded every day with an average value of 9.518 ± 0.377 ppm mV^{-1}. Samples were normalized to Vienna Pee Dee Belemnite (VPDB) and Vienna Standard Mean Ocean Water/Standard Light Antarctic Precipitation (VSMOW/SLAP) by an external standard mixture of 16 *n*-alkanes with $\delta^{13}C$ values that range from −25.9‰ to −33.7‰ and δD values from −17‰ to −256‰ (A6 mix obtained from A. Schimmelmann, Indiana University). The RMS error determined from replicate measurements of the standards run during the course of these analyses average 0.8‰ and 5.1‰ for $\delta^{13}C$ and δD, respectively, and constitute uncertainty in terms of accuracy. Replicate measurements of individual analytes average 0.2‰ and 3‰ for $\delta^{13}C$ and δD, respectively, and constitute measurement precision. Corrections were made for the methyl group added during methylation for the *n*-alkanoic acids ($\delta^{13}C$ of −24.7 ± 0.2‰ and δD of −186.9 ± 3.7‰) by mass balance.

2.6. GDGT Analyses

An internal C_{46} GDGT standard (Huguet et al., 2006) was added to the polar fractions containing glycerol dialkyl glycerol tetraethers (GDGTs) for quantification. These fractions were then dissolved in hexane: isopropanol (99:1) and filtered (0.45 μm PTFE) prior to injection on an Agilent 1260 High-Performance Liquid Chromatography (HPLC) coupled to an Agilent 6120 mass spectrometer at the University of Arizona. GDGTs were analyzed using two BEH HILIC silica columns (2.1 × 150 mm^2, 1.7 μm; 90 Waters) and the methodology of Hopmans et al. (2016). Single ion monitoring (SIM) of the protonated molecules ($M + H^+$ ions) was used to detect and quantify GDGTs with abundances determined by comparison to an internal standard at *m/z* 744. We report total (Σ) concentrations of branched (brGDGTs) and isoprenoidal (isoGDGTs) GDGTs in the sediments as measures of terrestrial and marine inputs, respectively, and calculate the branched and isoprenoidal tetraether (BIT) index:

$$BIT = \frac{Ia + IIa + IIa' + IIIa + IIIa'}{Ia + IIa + IIa' + IIIa + IIIa' + Cren} \tag{4}$$

where Ia, IIa, and IIIa represent the abundances of both the 5′ and 6′ methyl isomers of the noncyclic terrestrial brGDGTs (from soil acidobacteria) and Cren represents the abundance of crenarchaeol (mostly produced by marine archaea) (Hopmans et al., 2004).

In all samples, the 5-methyl brGDGT index, MBT'_{5Me} (de Jonge et al., 2014; Hopmans et al., 2016) was calculated as

$$MBT'_{5Me} = \frac{Ia + Ib + Ic}{Ia + Ib + Ic + IIa + IIb + IIc + IIIa} \quad (5)$$

and converted to MAAT using the BayMBT calibration (Dearing Crampton-Flood et al., 2020). For the prior distribution, we used a mean of 10 ± 15°C based on the mean summer temperature of 10°C estimated from the S-index from the same sites (Passchier et al., 2017) which is supported by pollen assemblage MAAT estimates below 12°C (Macphail & Truswell, 2004; Truswell & Macphail, 2009).

In addition, the cyclization of branched tetraether (CBT′) index (De Jonge et al., 2014) was calculated and utilized to estimate soil pH.

$$CBT' = log_{10}\left[\frac{Ic + IIa' + IIb' + IIc' + IIIa' + IIIb' + IIIc'}{Ia + IIa + IIIa}\right] \quad (6)$$

$$pH = 7.15 + 1.59CBT' \quad (7)$$

IsoGDGTs with 0–3 cyclopentane moieties (GDGT-0 to GDGT-3) and crenarchaeol (Cren) with an additional cyclohexane moiety and its regioisomer crenarchaeol′ (Cren′) are dominantly from marine archeal production. Following Schouten et al. (2007), TEX_{86} was calculated using the equation:

$$TEX_{86} = \frac{[GDGT-2] + [GDGT-3] + [Cren']}{[GDGT-1] + [GDGT-2] + [GDGT-3] + [Cren']} \quad (8)$$

We converted the TEX_{86} record to mean annual sea surface temperatures (SSTs) using the BAYSPAR calibration (Tierney & Tingley, 2014). For the prior distribution, we used 15 ± 10°C based on SST estimates of 22°C–12°C from the late Eocene to post-EOT from Maud Rise (Petersen & Schrag, 2015) and on mixed layer planktic foraminifera (*Chiloguembelina cubensis*) from Kerguelen Plateau Sites 738 and 744 with $\delta^{18}O$ values that indicated temperatures between 5°C and 10°C (Zachos et al., 1994). Similar temperatures are also suggested in the region based on modeling of ocean temperatures aligned with temperature reconstructions from further afield (La Meseta formation, Seymour Island, Antarctic Peninsula) using clumped isotopes on bivalve shells and TEX_{86} (Douglas et al., 2014).

Samples with a BIT > 0.4 were excluded from ocean temperature estimates. In addition, samples with a delta ring index (ΔRI) > 0.3 were excluded as a high ΔRI implies nonanalog distributions, following (Zhang et al., 2016):

$$RI_{\text{sample}} = \left(0[GDGT-0] + 1[GDGT-1] + 2[GDGT-2] + 3[GDGT-3] + 4[cren] + 4[cren']\right) \quad (9)$$

$$RI_{TEX} = -0.77TEX_{86} + 3.32\left(TEX_{86}\right)^2 + 1.59 \quad (10)$$

$$\Delta RI = RI_{\text{TEX}} - RI_{\text{sample}} \quad (11)$$

3. Results

In generating a new microfossil and biomarker multiproxy study of conditions in East Antarctica before the onset of the EOT, we revisit cores that have been studied for several mineralogical and inorganic geochemical weathering proxies. The Prydz Bay, late Eocene to Oligocene sedimentary sequence has previously been described by Passchier et al. (2017). The results of our organic multiproxy study are reported on that lithostratigraphic framework in the supplementary information (Figures S2 and S3). The results of this organic

study are presented on the age scale here (Figure 3), alongside summary contextual information about the regional erosion context and marine depositional type (Figures 3a and 3b).

3.1. Pollen

Palynological assemblage recovered include some penecontemporaneous angiosperm (mostly *Nothofagus*), gymnosperm, and spores, along with a dominating reworked assemblage composed mostly of taeniate bisaccate pollen and spores (e.g., *Protohaploxypinus* spp., *Striatopodocarpidites* spp, *Lunatisporites pellucidus, Playfordiaspora crenulatus,* and *Triplexisporites playfordii*) of Permian and Permo-Triassic transition age. Most of the bisaccate pollen recovered have a diagnostic "taeniate" (striped) appearance due to ridges on the wall of the central structure, many of these forms are related to Glossopteridales (extinct seed plants) common during the Permian on Gondwana. Glossopteridales pollen was also found in a terrestrial coal sample from Lamping Peak, Central Transantarctic Mountains, Antarctica, which we tested as a potential source rock for the reworked material delivered to Prydz Bay.

Examining the penecontemporary pollen assemblage in the Prydz Bay sediments (Figure 3c), we find *Nothofagus* to be dominant (mean 56%, $1\sigma = 18\%$, $n = 39$), with a secondary presence of gymnosperms, and lesser amounts of spores and angiosperms (other than *Nothofagus*). *Nothofagus* proportions peak at 84% at 35.7 Ma and decrease to an average of 54% ($1\sigma = 17\%$, $n = 33$) across 35.7 to 32.9 Ma. At 34.1 Ma, gymnosperm pollen reaches 55%, their highest proportions. While there are temporary declines in the dominance of *Nothofagus* after 34.7, 34.3 and 33.6 Ma, their proportions recover afterward, suggesting that the surviving vegetation remains a *Nothofagus*-gymnosperm mixture. Penecontemporary pollen grains are well preserved, with light-colored grains indicating the absence of thermal alteration.

Penecontemporaneous pollen concentrations average 2×10^3 count/gdw and peak at 12.2×10^3 counts/gdw at 35.7 Ma, when they exceed reworked pollen abundances, suggesting a flourishing ecosystem (Figure 3d). Penecontemporary pollen counts then decline by two orders of magnitude to an average of 745 counts/gdw indicating deteriorating conditions for plants.

Reworked pollen concentrations average 5×10^3 count/gdw and exceed penecontemporary pollen (by 1- to 60-fold) in almost all samples after 34.7 Ma (Figure 3d). In one sample at 34.8 Ma with anomalously low concentrations of reworked pollen grains, microscopy reveals charcoal or coal fragments, likely also signals of reworking (marked with an asterisk on Figures 3 and S3). Although there are variable concentrations of reworked pollen throughout the record, there is an abrupt increase in reworked pollen concentration at 33.6 Ma to peak concentrations in the record that coincides with major depositional system change to diatomaceous mudstones and massive diamictite at the Eocene Oligocene Glacial Maximum (EOGM; Figure 3b). Reworked concentrations increase after the EOT and peak at 12.6×10^3 counts/gdw at 33.5 Ma (Figure 3d).

3.2. Plant Wax

3.2.1. Abundance

We quantified individual *n*-alkanoic acids with C_{16}–C_{30} chain length (data set: Tibbett et al., 2021). The *n*-alkanoic acids are co-dominated by C_{16} and C_{18} compounds, common in many marine and terrestrial organisms and long-chain *n*-alkanoic acids with an even over odd predominance characteristic of terrestrial higher plants. Summarizing the molecular abundance distributions of the long-chain C_{24}–C_{30} *n*-alkanoic acids presumed to derive from plant wax sources, we calculate their summed concentration (Σ_{acid}) averaging 8.5 ± 2.7 μg/gdw (Figure S3), with a mean ACL of 26.4 and CPI of 5.89 (range 3.8–6.9). The lowest CPI of 3.8 is found at 34.8 Ma corresponding to low concentrations of Σ_{acid} (1.39 μg/gdw). The *n*-alkanoic acid fraction has a clean baseline, high CPI, and long ACL and is interpreted to represent penecontemporaneous inputs, from marine and terrestrial production, and we therefore focus on the *n*-alkanoic acids for compound-specific isotopic analyses, similar to prior work in Antarctic marginal sediments of Miocene and late Eocene age in the Ross Sea and Antarctic Peninsula respectively (Feakins et al., 2012, 2014). In particular, we select the C_{30} *n*-alkanoic acid as most likely indicative of terrestrial plant sources based on molecular abundance and carbon isotopic differentiation of sourcing between mid- and long-chain *n*-alkanoic acids (see Figures S5 and S6).

We quantified individual *n*-alkanes with C_{17}–C_{29} chain length. Many samples contained short to mid-chain *n*-alkanes in equal or greater abundance to the longer chains, a common symptom of thermal maturity. Specific signs of maturation include a modal *n*-alkane shorter than C_{23}, with short-mid chain *n*-alkanes having a CPI ~ 1, emerging above an uncharacterized complex mixture (UCM; see Figure S4). All Prydz Bay alkanes fractions contained substantial UCMs and short-chain alkanes, except for one sample with a typical plant wax distribution in Site 1166, during the peak warmth at 35.7 Ma. For the long-chain C_{23}–C_{29} *n*-alkanes, presumed to derive from plant waxes, we calculated a mean ACL of 25.5 and CPI of 3.7 (range 1.7–4.6), and Σ_{alk} was 2.1 ± 0.6 μg/gdw, a quarter of the Σ_{acid} concentrations. Given the low abundance of long-chain *n*-alkanes and signs of maturity noted here and previously in these Prydz Bay sediments (Kvenvolden et al., 1991), we suspect that at least some of the *n*-alkanes are thermally mature. We expect these are reworked mixtures from earlier sedimentary deposits, rather than in situ alterations given the co-occurrence with *n*-alkanoic acids that are incompatible with thermal alteration.

Within the alkane fraction, we detected hopanes, bacterial membrane lipids that are used as thermal maturity markers (Inglis et al., 2020). We found hopanes in the alkane fractions of all Prydz Bay sediments, including the most mature samples (high abundance of short-chain *n*-alkanes with low CPI, UCM and no alkanes > C_{25}) from the coal-rich layer. C_{27}, C_{29}, $C_{30,}$ and C_{31} hopanes were identified (Figure S4). We focused on the C_{31} hopane which is the most commonly reported and determined ratios of ββ/(αβ+βα+ ββ) averaging 0.45 ± 0.07, indicating moderate thermal maturity in glacio-fluvially eroded sediments. Downcore variations indicated elevated maturity in the coal-bearing sample (0.34) and lower maturity (0.57–0.76) in the warm intervals (Figure S3).

We obtained a potential source rock, a Permian coal sample, for comparison to the reworked alkanes. Corroborating the interpretation of reworked *n*-alkanes in the Prydz Bay sediments, the terrestrial, pollen-bearing coal sample yielded low abundances of mature, short- to mid-chain (CPI ~ 1) *n*-alkanes. Homologs detected above the UCM range from C_{18} to C_{29}, short chains dominate (with a CPI ~ 1) and the modal chain length *n*-alkane was C_{20} (52 ng/gdw). Corroborating the interpretation of penecontemporary *n*-alkanoic acids, these were below detection levels in the Permian coal. This is as expected as coals typically contain mature *n*-alkanes that are the product of thermal alteration, whereas fatty acids are considered more labile and would be altered and lost during coalification. We did not find hopanes in the terrestrial Permian coal sample, but its alkanes are at very low concentrations, and thus we infer that hopanes are below the detection limit or poorly preserved.

3.2.2. Compound Specific Isotopic Analyses

The δD of the C_{24}, C_{26}, C_{28}, and C_{30} *n*-alkanoic acids had an average value of −239‰ (range −280‰ to −164‰), −257‰ (range −287‰ to −216‰), −232‰ (range −269‰ to −196‰), and −222‰ (range −245‰ to −206‰). Due to microbial production of *n*-alkanoic acids which has been evaluated in Antarctic glacial lakes previously (Chen et al., 2019), and consistent with $\delta^{13}C$ values (reported below and Figure S5), we assume the C_{30} best represents a plant wax source, hereafter δD_{wax}. The downcore record of δD_{wax} (Figure 3h) shows that there is a trend toward D-enrichment up section. The most depleted value is in the oldest sample at 35.8 Ma and the most enriched value occurs at 33.3 Ma. δD_{wax} record indicates large variability before and during the EOT with fluctuations as high as 30‰ from 35.2 to 35.0 Ma. At the EOT, there is a high of −208‰ for δD corresponding to a 20‰ increase from 33.8 to 33.5 Ma.

We found that the C_{24}, C_{26}, C_{28}, and C_{30} *n*-alkanoic acids had a mean $\delta^{13}C$ value of −25.5 (range −27.2‰ to −24.4‰), −25.6 (range −27.1‰ to −24.9‰), −27.3 (range −28.2‰ to −25.6‰), −29.7‰ (−31.7‰ to −28.5‰). The tendency is to ^{13}C-depletion in longer chain lengths (see Figures S5 and S6). Microbial inputs of *n*-alkanoic acid may be present in the shorter chain lengths as indicated by their more enriched values as previously noted in Antarctic lakes (Chen et al., 2019); therefore, we report and discuss $\delta^{13}C$ of the C_{30} *n*-alkanoic acid, hereafter $\delta^{13}C_{wax}$. Across the Prydz Bay record, there is no temporal trend in the $\delta^{13}C_{wax}$ record; however, from 35.3 to 34.9 Ma, there is a 1.8‰ positive shift followed by a 2.4‰ decrease in $\delta^{13}C_{wax}$ at 34.7 Ma (Figure 3g). After this event, $\delta^{13}C_{wax}$ increases into and across the EOT reaching a maximum of −28.6‰ after the EOT at 33.6 Ma. There is a decrease in $\delta^{13}C_{wax}$ around 33.3 Ma from −28.9‰ to −31.3‰ before returning to the baseline of ~ −29.0‰. The $\delta^{13}C$ of the C_{30} *n*-alkanoic acid ranged from −31.9‰ to −28.6‰, with a 3.3‰ positive trend across the Prydz Bay record.

3.3. GDGTs

ΣbrGDGTs had an average concentration of 42 ng/gdw with a range of 9–154 ng/gdw. The maximum concentrations correspond to Site 1166 with values of 115–154 ng/gdw at 35.7 Ma (Figure S1). The rest of the record from Sites 742 and 739, the brGDGT concentrations remain lower than 100 ng/gdw. For all samples, we calculated MBT'_{5Me} and used BayMBT calibration to estimate MAATs over the adjacent continent between 8°C and 20°C. We found soil pH, based on CBT′, spanned pH 5.7 at 37.5 Ma to 6.7 at 33.5 Ma with a step increase at 33.7 Ma from pH 6.1–6.5.

ΣisoGDGTs had an average concentration of 150 ng/gdw with a range of 12–730 ng/gdw (Figure 3e). Site 1166 had the highest concentrations with 730 ng/gdw at 35.7 Ma. Site 742 had an initial increase in ΣisoGDGT concentration from 25 to 109 ng/gdw that overlaps with an increase from Site 1166 (35.8–35.7 Ma). In the rest of the record, there were notable increases in the ΣisoGDGTs from 39 to 266 ng/gdw at site 742 at 35.0 Ma, from 21 to 344 ng/gdw at site 739C at 34.7 Ma, and values remained above 100 ng/gdw starting at 33.7 Ma and reaching a maximum of 515 ng/gdw at 33.6 Ma and of 526 ng/gdw at 33.4 Ma. The lowest concentrations reached after 33.7 Ma are 178 ng/gdw at 33.1 Ma and 126 ng/gdw at 32.9 Ma.

BIT values ranged between 0.2 (marine-dominated) and 1.0 (terrestrial-dominated), however, most samples were terrestrially dominated precluding ocean temperature reconstructions. A few samples have low BIT, and that change is driven by increased marine productivity as denoted by ΣisoGDGT abundance spikes. In the Southern Ocean, GDGT-1, -2, and -3 are minimal, and distributions are dominated by GDGT-0 and crenarchaeal (Zhang et al., 2016) this can lead to a loss of sensitivity in the coldest waters (Tierney & Tingley, 2015), however with TEX_{86} of 0.4–0.6 in these late Eocene samples, temperature estimates from these samples are likely to be robust. The ΔRI ratio allows us to check for normalcy of the distributions obtained for the isoGDGTs. The ΔRI ranged from 0.14 to 1.44 and denoted samples where the TEX_{86} estimates would be biased by distributions outside those known for the modern ocean. For samples with BIT < 0.4 and ΔRI $<$ 0.3, TEX_{86} values were used to estimate ocean temperatures using the BAYSPAR calibration finding temperatures from 8°C to 14°C ($n = 6$), most of the samples were dominated by terrestrial signals such that ocean temperatures could not be obtained.

4. Discussion

4.1. Excluding the Permian Influence in Late Eocene Sediments

When reconstructing vegetation from these Prydz Bay sediments, we find a large and variable proportion of reworked pollen and spores of primarily Permian age, although a few Cretaceous angiosperms were recovered as well. The majority of the palynological yield is composed of extinct seed plant's bisaccate taeniate grains related to Glossopteridales, spores, and other Permian to Permo-Triassic transition age species. These reworked palynomorphs are likely sourced from the Prince Charles Mountains along the Lambert Glacier-Amery ice shelf system. Within the Lambert Graben, there is a wide distribution of Permian sediment consisting of Permian coal and sandstone (Veevers and Saeed, 2008) with upper Permian coals within the Bainmedart Coal Measures that contain plant material including pollen, wood, leaves, and charcoal material from *Glossopterid* gymnosperms (McLoughlin et al., 1997).

Fluvial or glacial erosion of these Permian sediments likely explains the reworked Permian pollen detected in Prydz Bay cores (Figure 3d), with glacial erosion expected to explain the increased erosion of reworked pollen at and after the EOT (see Section 4.5). Before the erosive flux from marine-terminating glaciers detected in marine geochemistry at the EOT (Scher et al., 2011), there was an earlier glacial advance at the Priabonian Oxygen Maximum (PrOM) (Scher et al., 2014) with glacio-fluvial erosion (nonmarine terminating glaciers) with geochemical signals detected at the Kerguelen Plateau, before the start of this Prydz Bay record. After the PrOM, warm events would have melted glacial ice and led to fluvial erosion, and then the cirque mountain glaciers in the Gamburtsev Mountains (Rose et al., 2013) would have re-initiated and expanded as temperatures dropped. Thermochronometry provides constraints on this phase of erosion and suggests that while glaciers were still wet-based, before the EOT, they had their greatest erosive power (Tochilin et al., 2012). We expect that the climatic fluctuations and the erosive power of advancing ice, increased the erosion of ancient sediments (bearing pollen, alkanes, and more thermally mature hopanes). At 34.8 Ma (483.93 mbsf, Figure S3) there is a large input of coal and reworked pollen, in the nearest biomarker

sample (at 484.05 mbsf), we find no isoprenoidal or branched GDGTs detected, and very low amounts of long-chain *n*-alkanoic acids. This sample had the highest concentration of short- to mid-chain (C_{17}–C_{25}) *n*-alkanes (an order of magnitude above other samples), with a modal concentration in C_{18}, a low CPI, and no *n*-alkanes >C_{25} detected, consistent with alkanes from coal. We compared a sample of pollen-bearing (Warny, pers. comm.), Permian-age strata, from Lamping Peak in the Beardmore Glacier region of the Central Transantarctic Mountains (Flaig, pers. comm.) to assess possible reworking of organic proxies along with reworked pollen. The coal sample did not contain GDGTs or *n*-alkanoic acids, suggesting no ancient contributions to the brGDGT or isoGDGT proxies or the plant wax *n*-alkanoic acids found in Prydz Bay. The coal sample included mostly short-chain *n*-alkanes (<C_{25} *n*-alkanes) with no odd over even preference above an uncharacterized complex mixture, typical of thermally mature samples. The fraction included low abundances of long-chain *n*-alkanes from C_{25} to C_{29} with the expected odd over even dominance suggesting plant-derived distribution (including detectable amounts of the C_{29} *n*-alkane). Although Permian plant waxes are not well known, during the Permian, gymnosperms would have been the plants present and gymnosperms produce some *n*-alkanes (Diefendorf et al., 2015). Although peaks are barely above detection limits, it remains possible that erosion of Permian coals can contribute to the long-chain *n*-alkanes; therefore, we avoid this compound class for isotopic reconstructions in Prydz Bay. Furthermore, mature *n*-alkane distributions were found in Prydz Bay samples in this study as well as in the original reports (Kvenvolden et al., 1991). The coal sample did not yield long-chain *n*-alkanoic acids or brGDGTs; thus, we infer that these biomarkers and their isotopes reflect penecontemporaneous inputs into Prydz Bay.

Penecontemporary pollen in the Prydz Bay sediments can be readily differentiated from reworked pollen, based on their taxon identification, surface features (specifically the Permo-Triassic "taeniate" features described previously for the reworked grains), and preservation (with good preservation for the penecontemporary pollen) and low thermal maturity (light-colored grains). Species present include *Nothofagus* and other angiosperms in small amounts, gymnosperms (likely *Podocarpus*), and some spores. Spore concentrations are low and we note that mosses are extant on Antarctica in the more humid regions such as the Antarctic Peninsula, whereas other plants are locally extinct. The plant community of the late Eocene is low diversity and its composition does not appreciably change across the 3 Myr period including the EOT, suggesting that southern beech-podocarp tundra assemblages were the last surviving vestiges of forests of the same composition.

Like the pollen, the biomarkers in the same sediments also carry components of penecontemporary and reworked contributions that can be differentiated. We do not suspect any thermal alteration of the *n*-alkanoic acids due to their "fresh" molecular abundance distributions. Variability in δD values between chain lengths and downcore (Figure S5), would also tend to be lost during any thermal alteration that drives H-exchange (Schimmelmann et al., 2006), thus variable δD values further support our interpretation of penecontemporary and not reworked *n*-alkanoic acids.

We avoid low abundance, mature alkanes as they are unlikely to be penecontemporary, and as they may have undergone H-exchange during maturation. Given their low abundance, they are unlikely to be useful indicators of reworking (unlike the reworked pollen), with the exception of one sample at 34.8 Ma, which has the highest abundance of short- and mid-chain *n*-alkanes, no chain lengths >C_{25}, an uncharacterized complex mixture, and this is the same sample where microscopy identified substantial coal or charcoal—likely a deposit of a remobilized coal eroded from land. Reworked *n*-alkanes have also been reported in Neogene age sediments on the Antarctic margin in the Ross Sea (Duncan et al., 2019). The presence of thermally mature hopanes confirms the likely thermal alteration of the alkanes on land and remobilization by erosion, with mineral-associated alkanes and hopanes in sediments that had already lost alkanoic acids during maturation. We do not suspect in situ thermal alteration, given that the *n*-alkanoic acids have a fresh molecular abundance distribution as may be expected in unaltered marine sediments in a terrestrial margin setting.

Can the GDGTs be disturbed by reworking noted in the microfossil and alkanes fractions? By definition, the samples that have marine-dominated GDGT production are free from concerns of glacial erosion of terrestrial sediments. GDGT fractions with high terrestrial soil inputs (high BIT), likely derived from penecontemporary soils in the catchment. We exclude the possibility of reworked GDGT signals, on the basis that (1) the Permian terrestrial pollen-bearing coal sample contained no measurable br- or iso-GDGTs,

concentrations (below detection), and (2) we are aware of no prior reports of Permian GDGT preservation. Thus, these brGDGT biomarkers, and proxy information they contain, are less likely to be influenced by reworked sedimentary erosion than mineralogical proxies, for example, kaolinite in the clay size fraction has been shown to be a reworked mineral from earlier greenhouse climate states (Passchier et al., 2017).

4.2. Terrestrial Inputs and Marine Productivity at Continental Margins

The membrane lipid biomarkers of bacteria and archaea provide an indicator of terrestrial influx from soils and of marine productivity. Terrestrial versus marine influxes are commonly tracked via the BIT index and variations in the BIT index between the sites may be partly due to their proximity to shore, but any such differences are clearly overwhelmed by changes between lithological facies within each segment (Figure S1). The BIT variations instead reflect facies, responding to the changing depositional environment, the changing terrestrial export and marine productivity (Figure S2). Site 1166 is the shallowest site and closest to shore but sees a large shift in BIT associated with lithological changes. Site 742 has high and stable BIT values. Site 739 has similar BIT at the outset, despite being farthest offshore there is a shift from terrestrial to marine dominance at the EOT. As glaciers advance, shorelines could shift associated with glacial isostatic and eustatic changes (Hochmuth, Gohl, et al., 2020; Paxman et al., 2019); we would expect an initial regression followed by a transgression with more marine influence at this site (Stocchi et al., 2013). However, the BIT ratio here responds more to variations in the isoGDGT flux, and thus it may be more informative to look at the ΣbrGDGT and ΣisoGDGT concentrations independently (Figure S2). While ΣbrGDGTs are fairly invariant, there are interesting features in the ΣisoGDGT concentrations (Figure 3e) that suggest variations in marine productivity (Fietz et al., 2011).

4.3. Late Eocene Warmth Between PrOM and the EOT

Comparison data from the Kerguelen Plateau from the εNd in fossil fish teeth (Figure 3l) indicates two major glacial expansions, and corresponding erosion pulses, at 37.5 Ma for the PrOM (Scher et al., 2014) and at 33.7 Ma for the EOT (Scher et al., 2011). Between the PrOM and the EOT glacial expansions, oxygen isotopes in benthic foraminifera are generally <2.0‰ and fairly invariant indicating warmth and reduced ice volume lasting several million years (Figure 3k). In the available records from Prydz Bay, we find evidence for warm conditions on land and marine proxies with some abrupt (<50 ka) warmings at 35.7 and 34.7 Ma within the generally warm 2 million years from 35.7 to 33.7 Ma (Figures 3c–3j).

Using the BayMBT temperature proxy for soil biomarkers, we find late Eocene MAAT averages 14°C with a peak temperature of 20°C (a warming of 4°C above background) at 35.7 Ma (Figure 3f). Late Eocene warmth was previously identified by the weathering proxy (S-index), showing average temperatures of 10°C, and abrupt warming to peak temperatures of 12°C at 35.7 Ma (Passchier et al., 2017). During the warm spell at 35.7 Ma, we find the proportion of penecontemporaneous pollen increases to a maximum of 12×10^3 counts/gdw or 90% of all pollen (Figure 3d), much higher than elsewhere in the record (typically $<1 \times 10^3$ counts/gdw and <20%) suggesting a flourishing of plants in that warm interlude in particular among the *Nothofagus* species (Figure 3c). Both branched and isoprenoidal GDGT concentrations increase at that time suggesting a time period of high productivity. This warming event is also supported by the mineralogy of the Prydz Bay cores with kaolinite dominating (>50%) from 36 to 34.4 Ma (Figure 3b) (Forsberg et al., 2008). The additional independent temperature estimates from GDGTs and the pollen record adds additional evidence of a warming interval in the late Eocene around 35.7 Ma before the glacial transition.

Around 35.0 Ma, there is a gradual warming detected in the BayMBT which peaks at 17°C whereas the (cool-offset) S-index spikes to 12°C in what looks to be an abrupt warming (Passchier et al., 2017) and penecontemporary pollen inputs increase at 34.7 Ma to 3.5×10^3 counts/gdw. There is also an increase in δD_{wax} of 10‰ consistent with warming and/or drying. The timing of the warming is estimated by the linear age model to be ~34.7 Ma, but is not well constrained (Figure 2).

At the warm events at 35.7 and 34.7 Ma, we observe spikes in the ΣisoGDGT concentration suggesting marine production increases (though not as persistent as observed at the EOT). In these events, we find land plants flourish, chemical weathering increases, and soil bacterial lipid biomarkers indicate a 3–6°C rise in ambient air temperatures over ~100 ka for 35.7 Ma and a 3°C warming over ~500 ka for 34.7 Ma. The

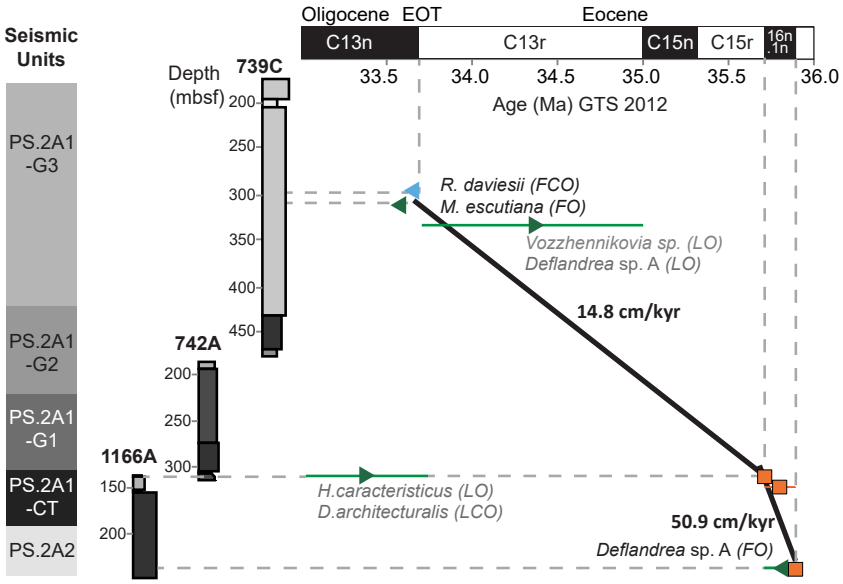

Figure 2. Age model for the Prydz Bay sedimentary sequence compiled from sections of 1166A, 742A, and 739C, with age datums based on biostratigraphy including first and last occurrence (directional triangles) of named nannofossils (blue) and dinoflagellates (green) and seismic tie points (orange squares) relative to GTS 2012 (Gradstein & Ogg, 2012). Chron 13n occurs within the early Oligocene, the remainder within the late Eocene, and the approximate timing of the Eocene-Oligocene transition (EOT) is denoted alongside the paleomagnetic boundaries for reference. Species labeled in gray are not used in the construction of the age model but are provided for context, tie points used to connect depth to age are illustrated with dashed lines. Diagram modified from Passchier et al. (2017) to show the linear fit age model (thick black line) and implied sedimentation rates.

rise in marine productivity in response to temperature increases, may suggest an increase in fluvial runoff and nutrient supply to the coast promoting marine production during warmer and wetter times for eastern Antarctica.

In the marginal setting, soil biomarkers inputs detected by the BIT and ΔRI preclude ocean temperature reconstructions in most samples. Contrasting available BAYSPAR estimates before and after the EOT at 34.2 and 33.5 Ma, we find SSTs cool by ~6°C from 14°C to 8°C (Figure 3f). The absolute values of these Prydz Bay SSTs are comparable to model estimates of <10°C for the Southern Ocean during the Priabonian (37.8–33.9 Ma, pre-EOT) conducted using the HadCM3L model at 4× preindustrial atmospheric pCO_2 (Inglis et al., 2015) as well as ocean temperature reconstructions estimating a 4°C cooling from 13°C to 9°C on the Falkland Plateau abased on UK'_{37} and TEX_{86} (Houben et al., 2019; Liu et al., 2009).

After the EOT, the Prydz Bay SSTs rebound slightly (to 10–12°C) between 33.3 and 33.2 Ma, and there is a small increase in penecontemporaneous pollen concentration. A post-EOT warming of 1–2°C was previously suggested in the Southern Ocean from the Kerguelen Plateau based on planktic foraminifera Mg/Ca (Bohaty et al., 2012).

4.4. Hydroclimate of the Late Eocene

We assessed plant wax abundance, $\delta^{13}C$ and δD (Figures 3g and 3h). The $\delta^{13}C$ of the C_{30} *n*-alkanoic acid ranged from −31.9‰ to −28.6‰, with a 3.3‰ positive trend which is much greater than the 0.4–0.6‰ reconstructed change in atmospheric $\delta^{13}C$ during the same time period (Tipple et al., 2010), suggesting an overall drying. The δD of the C_{30} *n*-alkanoic acid varied from −245‰ to −206‰, a c. 40‰ range. Across the EOT the δD_{wax} shifts from −233‰ to −209‰ (+24‰) from 33.7 to 33.5 Ma (Figure 3h). The hydrogen isotopic composition of plant wax records the isotopic composition of rainfall, subject to a large biosynthetic fractionation. The plant wax *n*-alkanes and *n*-alkanoic acids have been calibrated in a variety of grass, shrub, and forested ecosystems at high latitudes in the Arctic (McFarlin et al., 2019). The most relevant of these calibrations are those of plant wax *n*-alkanoic acids in a moss-conifer ecosystem archived in soils

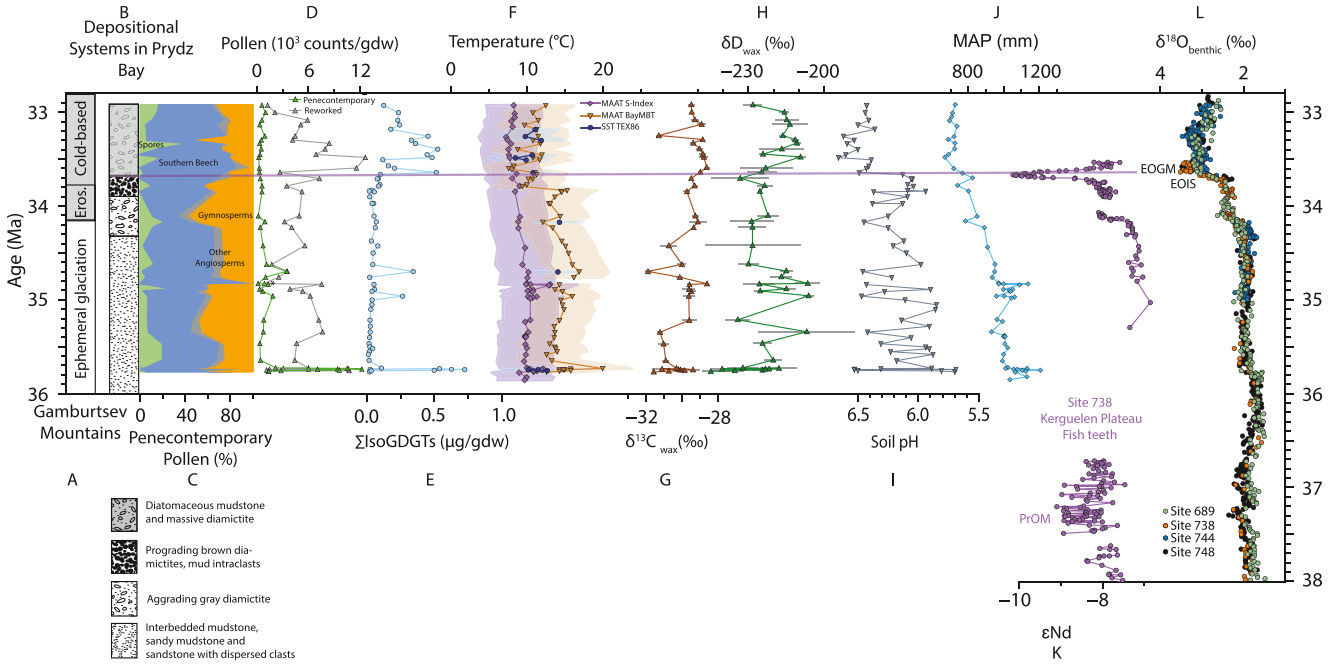

Figure 3. Multiproxy latest Eocene reconstruction from Prydz Bay showing (a) conditions in the Gamburtsev Mountains from ephemeral glaciation to accelerated erosion during glacial expansion to cold-based ice sheets at the EOT and (b) depositional systems inferred from Prydz Bay stratigraphy (both from Passchier et al. [2017] and references therein). Palynology results showing (c) penecontemporaneous pollen assemblage proportions and (d) total penecontemporaneous and reworked pollen concentrations. Biomarker results including (e) ΣisoGDGT concentrations as evidence for marine production (light blue circles), (f) and temperature estimates based on two soil-proxies for land conditions yielding MAAT estimates from the biomarker-based MBT'_{5me} with BayMBT calibration (orange downward triangles, this study) compared to the S-index weathering proxy (purple diamonds, Passchier et al., 2017), and limited ocean temperature estimates from the BAYSPAR calibration of TEX_{86} (dark blue circles). Plant wax records include (g) $\delta^{13}C_{wax}$ from the $C_{30\text{-acid}}$ (upward brown triangles), (h) δD_{wax} from the $C_{30\text{-acid}}$ (upward green triangles). (i) soil pH was reconstructed from CBT′. (j) MAP using the calibration of Sheldon et al. (2002) to the CIA-K weathering proxy from Passchier et al. (2017). For comparison, we show regional records of glacial ice volume and ice expansion based on (k) εNd in fish teeth (Scher et al., 2011, 2014) from ODP Site 738 (purple circles) as well as (l) $\delta^{18}O_{benthic}$ in Southern Ocean Sites 689, 738, 743, and 744 (Bohaty & Zachos, 2003; Bohaty et al., 2009; Cramer et al., 2009; Scher et al., 2014). Purple line highlights the diamict to diatomite depositional transition in Prydz Bay. CBT, cyclization of branched tetraether; EOT, Eocene-Oligocene transition; MAAT, mean annual air temperature; ODP, Ocean Drilling Program.

(Bakkelund et al., 2018) and archived in Greenland lakes (McFarlin et al., 2019) as they are the same compound class used here. However, plant wax hydrogen isotopic fractionations were not calibrated in austral plant communities that have been locally extinct from the continent of Antarctica for at least 15 million years (Warny et al., 2009). Although some of these late Eocene Antarctic species are today found in Tasmania and Patagonia, they have not yet been calibrated in terms of isotopic composition. However, a recent study of several temperate forest taxa in Chile (Cerda-Peña et al., 2020), reports *n*-alkyl lipid concentrations in *Nothofagus dombeyi*, and notes that *n*-alkanoic acids dominate over *n*-alkanes, unlike in most North American angiosperms, finding C_{22}–C_{32} *n*-alkanoic acids with the expected even over odd dominance and with the maximum abundance in C_{28}. This helps to establish *Nothofagus spp.,* represented in the pollen in Prydz Bay, as likely producers of the plant wax *n*-alkanoic acids in the same samples, given their similar molecular abundance distributions, with additional contributions expected from the gymnosperms.

Estimating δD_{precip} using the Arctic and globally-assessed fractionation of −99‰ (McFarlin et al., 2019) leads to estimates of δD_{precip} ranging from −162‰ to −104‰ across the Prydz Bay record. As expected, these values from the relatively warm Eocene are much more enriched compared to modern snow samples from glaciated Antarctica adjacent to Prydz Bay with snow samples from the East Antarctic Ice Sheet that range from −219‰ to −448‰ across an elevation transect of 1,040–4,093 m and from 46 to 1,183 km from the coast (Masson-Delmotte et al., 2008) (Figure 1a). The variability within the late Eocene record is not clearly mirroring other proxies in the reconstruction, and may represent variability in atmospheric conditions and thus precipitation isotopes, changes in plant communities and their fractionation or catchment sourcing in ways that are not presently understood, we thus do not interpret the variability in much of the plant wax record. Although it is not an abnormal shift among the variability in the record, there is a shift associated

with the EOT: δD_{precip} shifted from −149‰ to −122‰. This shift does appear to correspond to expected environmental changes. A similar 20‰ shift was estimated from the hydration waters of volcanic glass from the Sarmiento Formation, Patagonia (Colwyn & Hren, 2019). This shift occurs at the time of the ~+1.5‰ $\delta^{18}O_{benthic}$ shift identified from Kerguelen Plateau Sites (738, 744, and 748) at 33.7 Ma indicating enrichment in ^{18}O-seawater associated with glacial expansion. Globally a 1.5‰ increase in $\delta^{18}O_{benthic}$ is registered, 0.9‰ of this is thought to reflect a decrease in ocean bottom water temperatures (Lear et al., 2008) and 0.6‰ is a change in seawater due to the buildup of continental ice sheets. Based on the seawater change, and mass-dependent fractionation, we expect a D-enrichment in seawater of 5‰, which should lead to a commensurate 5‰ D-enrichment in meteoric water and plant wax. This would only explain part of the +20‰ shift, leaving the remainder as a sign of the enrichment of δD_{precip}. As we can rule out warming, based on numerous temperature reconstructions across the glacial expansion discussed previously, we infer the positive shift in δD_{precip} must represent increasing aridity, similar to interpretations of δD_{wax} in the latest Eocene records from the Antarctic Peninsula (Feakins et al., 2014). In the same location, corroborating information from increasing $\delta^{13}C$ of *Nothofagus* pollen grains was interpreted as signs of moisture stress in vegetation communities (Griener et al., 2013). Here too, aridity is also consistent with an increase in $\delta^{13}C_{wax}$ of +1.1‰ in conjunction with the increase in δD_{wax}. While there are additional possible influences on $\delta^{13}C_{wax}$ including atmospheric $\delta^{13}C$, estimates based on $\delta^{13}C$ of planktonic foraminifera suggest variations of no more than 0.4‰–0.6‰ in the latest Eocene (Tipple et al., 2010). We also find no evidence for a major change in vegetation assemblage, such as could drive a change in fractionation of either carbon or hydrogen isotopes. The vegetation is dominantly Southern beech (Figure 3c), with declining penecontemporaneous pollen abundances between a peak of 12.2×10^3 counts/gdw at 35.7 Ma with a steep decline and then low levels with the exception of 34.7 Ma (Figure 3d). A Student's *t*-test indicates a significant decline in penecontemporaneous pollen when comparing the record before and after the EOT; however, there is no strong change associated with the main ice expansion, instead the decline occurs with the earlier cooling and drying, detected by the mineralogical proxies after 35.7 and 34.7 Ma. The decline in pollen amounts indicates deteriorating conditions for tree growth, consistent with a cooling and drying climate.

Penecontemporary pollen concentration decreased by an order of magnitude from highs of 12×10^3 counts/gdw at 35.7 Ma to mostly $<1 \times 10^3$ counts/gdw thereafter with a low of 0.2×10^3 counts/gdw at 33.5 Ma (Figure 3d). Perhaps the strongest correlating change is to the mineralogical proxies showing a decline in MAP (Figure 3j) from a high of 1,200 mm to below 900 mm, as the penecontemporaneous pollen counts decline well before the EOT. MAP and penecontemporaneous pollen were observed to have a positive correlation ($r = 0.47$, $p < 0.05$) based on nonparametric methods that account for serial correlation (Ebisuzaki, 1997). MAP continues to drop to as low as 700 mm after the EOT as expected in a glacial climate state. These MAP estimates derive from the correlation to precipitation based on North American soils (Sheldon et al., 2002), as applied to the CIA-K index, a moisture responsive subset of the bulk detrital geochemical oxides that together are responsive to weathering. Previously the S-index, based on the molar ratio of Na_2O and K_2O to Al_2O_3, was used to infer gradual cooling from ~10°C before 35 Ma to a low of 7°C at 33.2 Ma (Passchier et al., 2017). As warm and wet conditions drive stronger weathering and cooler and drier conditions drive lesser weathering, these two proxies are related and moisture has a stronger correlation than temperature in the modern data set. We report both moisture and temperature interpretations here. The drying pattern can be compared to the soil pH estimates from the CBT′ index (Figure 3i), which shows a highly variable record in the late Eocene, with acidic conditions resulting from lowland soils during the warm and wet events described previously, as well as less acidic signals from drier conditions during colder times or upland locations as alpine glaciers initiate and expand in the catchment. In the late Eocene, the temperatures from the weathering proxy are cool-biased relative to the soil biomarker proxy, and experience a more gradual cooling trend. This may also reflect catchment sourcing with rock erosion in the Gamburtsev Mountains as glaciers grow. After the EOT, when ice sheets cover the upper catchments, the absolute temperature estimates are the same within uncertainties for the S-index and BayMBT (Figure 3f), suggesting a more consistent lowland source, with similar temperatures recorded.

4.5. Glacial Expansion at the EOT

Next, we examine the changes across the EOT recorded by several of the microfossil and biomarker proxies in Prydz Bay sediments (Figure 4), to assess their timing relative to glacial expansions of the EOIS detected

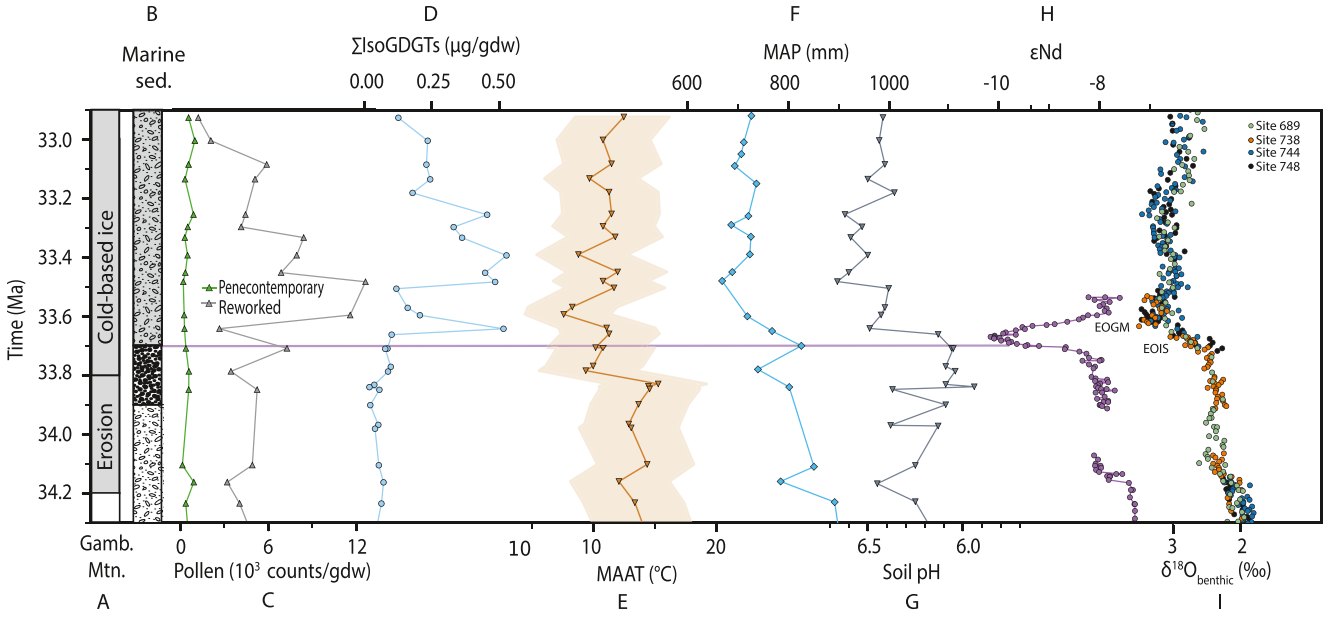

Figure 4. A detailed view of microfossil and biomarker evidence for change in East Antarctica across the EOT. (a) Glacial conditions in the Gamburtsev Mountains and (b) Prydz Bay stratigraphy (legend as in Figure 3), (c) pollen concentration (counts/gram of dry sediment), (d) ΣisoGDGT concentration, (e) BayMBT based MAAT, (f) MAP from CIA-K index, (g) soil pH, and comparison to (h) Kerguelen Plateau εNd records from Site 738 (Scher et al., 2011) and (i) $\delta^{18}O_{benthic}$ (sources as in Figure 3). Labels indicate EOIS (glacial expansion) and EOGM (formerly Oi-1; glaciation) features in (i) Purple line highlights the diamict to diatomite depositional transition in Prydz Bay. EOT, Eocene-Oligocene transition; MAAT, mean annual air temperature.

in the $\delta^{18}O_{benthic}$ (Hutchinson et al., 2021). For context from prior work in the region, Apatite Fission Track dating indicates maximum erosion from 34.2 to 33.8 Ma (Tochilin et al., 2012) across the EOIS as glaciers incised and eroded the formerly fluvial drainage basin of Gamburtsev Mountains and the Lambert Graben into the sediments of Prydz Bay, before cold-based glacial conditions were established at 33.8 Ma (Rose et al., 2013; Passchier et al., 2017, Figure 4a). Depositional systems in Prydz Bay transition from prograding diamictites to diatomaceous sediments a little later at 33.7 Ma (Figure 4b). Further offshore, the Kerguelen Plateau receives the εNd signal of glacial surge associated with EOT-1 and -2 (Figure 4h; Scher et al., 2011), and the glacial ice volume and cooling of bottom waters are reflected in the benthic oxygen isotope record (Figure 4i).

Here, we find the persistence, but low abundance, of penecontemporary pollen across the full EOT (Figure 4c), suggesting southern beech/podocarp vegetation were already restricted to refugia and were not eliminated as glaciers advanced to maximal extent at the EOGM (formerly Oi-1). The glacial surge of EOIS led to an increase in erosion of reworked pollen at 33.7 Ma and then a peak (12×10^3 counts/gdw) from 33.6 to 33.5 Ma perhaps indicating maximum glacial erosion, with sustained erosion of reworked pollen through 33.1 Ma.

Soil biomarkers indicate that MAAT cooled by 6°C abruptly at 33.8 Ma from an average of ~14°C before to 8–10°C thereafter (Figure 4d). This cooling occurred ~100 ka before the main inflection in the marine oxygen isotope curve of the EOIS, indicating that cooling of the catchment in East Antarctica preceded the continental-scale glacial ice volume and bottom water cooling. This makes sense as the Gamburtsev Mountains were the locus of glacial initiation (Rose et al., 2013) with valley glaciers descending via the Lambert Graben (Tochilin et al., 2012), which would have cooled the local catchment, before the continent-wide signals detected in the deep sea. The timing of the cooling appears earliest in the mineralogical proxies, which likely carry higher elevation erosion signals, and then abruptly in the soil biomarkers at the same time as glacial reconstructions suggest a shift to cold-based glaciers, suggesting ice-albedo feedbacks led to further cooling, including the lowland reaches of the catchment. The magnitude of this cooling is consistent with climate model experiments, that decrease carbon dioxide concentrations from 750 ppmv pre-EOT and 560 ppmV post-EOT to achieve EOT cooling and suggest a drop of 5°C across the EOT using the 2011 GENESIS

3.0 GCM combined with a BIOME4 equilibrium vegetation model (Feakins et al., 2014). This cooling incorporates responses to the decrease in atmospheric CO_2 as well as the ice-albedo feedback.

The soil biomarkers further indicate that cooling was accompanied by drying. Soil pH shifted from 6.0 to 6.5, with less acidic soils denoting reduced plant and microbial activity to acidify the soil and known to be consistent with drying. The shift is abrupt and may be linked to abrupt changes in climate and/or erosion associated with the abrupt expansion of the cryosphere (Figures 4h and 4i). Quantitative estimates of a reduction in mean annual precipitation can be calculated from the detrital mud geochemistry (CIA-K index, Passchier et al., 2013) using the calibration of Sheldon et al. (2002) to suggest gradually declining MAP from 900 to 700 mm across the EOT from 34.2 to 33.5 Ma.

These reconstructions constitute some of the few estimates for terrestrial conditions in the latest Eocene and add to the available evidence for proxy-model comparisons (Deep-MIP-EOT; Hutchinson et al., 2021). While the four climate models used different forcing and geography and diverge greatly in their absolute temperature in the interior of the Antarctic continent, their marginal temperature estimates for the pre- and post-EOT simulations are fairly consistent with each other. In their proxy-model comparison, they showed no proxy data from Antarctica, suggesting that their Antarctic predictions are untested and that this constitutes some of the first proxy constraints on absolute and relative temperature change to validate climate model experiments for the greenhouse-icehouse transition. Their climate model ensemble estimated a 3°C surface air temperature cooling at the edge of the Antarctic continent, which is the same (within uncertainties) as the magnitude of cooling observed, from both MAAT over land (from brGDGTs) and SSTs (from TEX_{86}) from our biomarker reconstructions using their broad integration windows pre- and post-EOT.

If we compare our two temperature proxies in Prydz Bay sediments in detail, the soil biomarker-based cooling and drying is larger and more abrupt than reconstructed from weathering proxies and this may reflect the differences in the catchment sourcing of organic and inorganic proxies. The biomarker approach finds a step cooling of 6°C within 50 ka at 33.8 Ma, whereas the weathering proxy records a cooling of half that magnitude gradually across 1 million years. The organic proxy records a step-shift in soil pH whereas the weathering proxy records gradual change. These offsets may reflect the different response times of soil organic microbial activity and parent rock weathering rates, or differential organic-inorganic sourcing from the drainage basin to the offshore archive. Catchment studies elsewhere show that erosion rates tend to have upland dominance (Scher et al., 2014; van de Flierdt et al., 2008), leading to expectations of a cold bias for the site of deposition. Early erosional and mechanical weathering signals are recorded for the inorganic proxies due to upland alpine glaciation (Rose et al., 2013). In comparison, lowland dominance is broadly reported in catchment studies of biomarkers (Freymond et al., 2018; Galy et al., 2011) based on areal extent and degradation in transit; therefore, a more proximal and rapidly responding biomarker signal is expected as conditions change. Whereas inorganic weathering proxies track aggregate conditions in the entire catchment, including uplands, biomarkers may not record the early phases of alpine glaciation. However, as ice sheets expand, the ice-albedo and ice-elevation feedbacks would have altered the local climate, including the lowlands, more strongly. The abrupt biomarker and microfossil changes recorded in Prydz Bay (Figure 4) appear to coincide with geochemical evidence for a glacial surge at EOIS recorded in εNd at the Kerguelen Plateau that marks the influence of the expanding EAIS on ocean chemistry (Scher et al., 2011), however additional corroboration of the relative timing of landscape and erosional shifts would benefit from those analyses in the same sediments. Between 33.8 and 33.7 Ma, εNd decreases by around 2.5 (Figure 4h) indicating glacial erosion of radiogenic rocks influencing marine chemistry with a small precursor and the main EOIS detected with timing matching that of the $\delta^{18}O_{benthic}$ record of glacial ice volume expansion and deep ocean cooling (Figure 4i).

A change in marine productivity also occurs in the ocean waters of Prydz Bay. We find sedimentary concentrations of ΣisoGDGTs are an order of magnitude more abundant after 33.7 Ma compared to consistently low abundances before (Figure 4d). This increase in marine archeal productivity corresponds to a major depositional system change from prograding diamictite to diatomaceous mudstones (Figure 4a) at EOIS (Figure 4i). Increased diatom productivity along with other changes in marine ecosystems are reported around the Southern Ocean at the EOT (Houben et al., 2013). The detected marine ecological shift and productivity increase at the EOT in Prydz Bay may be a response to regional ocean circulation changes with enhanced upwelling and sea ice formation (Houben et al., 2019), resulting in enhanced overturning,

resulting in changing bottom water (Figure 4i). Climate model experiments show that an increase in sea ice, following cooling linked to atmospheric carbon dioxide changes, could stimulate deep water production and Southern Ocean circulation (Goldner et al., 2014). Local effects from the glacial surge detected in the Kerguelen Plateau (Figure 4h), may have also locally stimulated increased marine productivity in Prydz Bay, as marine-terminating glaciers in Greenland today are noted as sources of nutrients that increase marine productivity (Meire et al., 2017). However, the glacial surges of EOIS (Figure 4g) predate the main marine productivity increase (Figure 4c) which appears to coincide with EOGM and glacial volume, suggesting the connection to a larger regional phenomenon associated with sea ice and ocean overturning. Changes in ocean circulation associated with the transition to icehouse conditions may explain the fertilization of marine productivity that continues well beyond the glacial erosion surge. It then follows that a slight decrease in ΣisoGDGT concentrations occurs at 33.2 Ma, associated with a reduction in EAIS size (Galeotti et al., 2016) visible in the oxygen isotope record (Figure 4i), presumably linked to reduced sea ice formation and ocean overturning. This is consistent with evidence for 1–2°C of warming based on planktic foraminiferal Mg/Ca from the Kerguelen Plateau (Bohaty et al., 2012). Locally we find Prydz Bay SSTs warm slightly to 10–12°C (Figure 4e) between 33.3 and 33.2 Ma, and there is a small increase in penecontemporaneous pollen concentration including spores suggesting slightly wetter conditions (Figure 4c) associated with regional oceanic changes and the reduction in EAIS extent.

5. Conclusions

Latest Eocene sediments from ODP Sites 739, 742, and 1166, from Prydz Bay, Antarctica encompassing the late Eocene through the EOT, provide records of both terrestrial and marine climate change. Prior mineralogical evidence from Prydz Bay indicates a gradual cooling and drying in the catchment since the last warm pulse at 34.7 Ma (Passchier et al., 2017). The East Antarctic Ice Sheet began with cirque glaciers in the Gamburtsev Mountains (Rose et al., 2013), with maximum erosion via the Lambert Graben as ice sheets surged (Tochilin et al., 2012), before the transition to cold-based glaciers as glaciation proceeded. Prior geochemical evidence from further offshore in the Kerguelen Plateau indicates marine-terminating glaciers reach the coastline by 33.7 Ma.

In the lead-up to the icehouse transition, the biomarker and pollen results from this study support the presence of a 3–6°C warming in the late Eocene at 35.7 Ma, followed by another warm spike at 34.7 Ma before the beginning of the EOT. The presence of penecontemporary pollen during and after the EOT suggest southern beech/podocarp vegetation refugia, with a vegetation community struggling to survive, as noted by concentration in pollen decreasing from 3.5 x 10^3 counts/gdw during the warm pulse at 34.7 Ma declining to ~0.4×10^3 counts/gdw before and during the EOT. The declines in penecontemporary pollen correlate with mineralogical evidence for cooling and drying in the catchment. The plant wax shifts in δD and $\delta^{13}C$ (+20‰ and +1.1‰) also suggest an increase in aridity, showing signs that drying was felt by plants. The biomarker proxies record an abrupt cooling 100 ka before the EOT, with terrestrial brGDGTs showing a MAAT decrease of 6°C, with a commensurate magnitude of cooling of SSTs based on available TEX_{86}. The same soil biomarkers also show an abrupt drying accompanied that cooling (based on soil pH). The soil biomarker transition is notably more abrupt and later than the catchment mineralogical evidence likely reflecting differences in catchment averaging of the two signals with earlier upland cooling detected in the rock-derived signal and lowland change occurring later as detected in the soil biomarkers. Marine biomarkers detect cooling of SSTs from 14°C to 8°C associated with the EOT, although the timing of the SST drop is poorly resolved as high terrestrial inputs obscure the proxy record in many samples with high BIT in this marginal setting. The ΣisoGDGT concentrations are a compelling aspect of the biomarker contribution to the Prydz Bay reconstructions, they indicate increased marine productivity after the EOT suggesting increased nutrient supply into the Southern Ocean with intensification of ocean circulation at the EOT.

Conflict of Interest

The authors declare no financial conflicts of interests for any author or their affiliations.

Data Availability Statement

Data files are archived at the NOAA paleoclimatology database at https://www.ncdc.noaa.gov/paleo/study/32052 (Tibbett et al., 2021).

Acknowledgments
This study was funded by the U.S. National Science Foundation NSF-OPP-1908548 to Sarah J. Feakins, NSF-OPP-1908399 to Howie D. Scher, and NSF-OPP-1743643 to Sandra Passchier. This study used samples and/or data collected by the International Ocean Discovery Program, supported by funding from the U.S. National Science Foundation and other member nations. The authors thank Peter Flaig for providing a sample of Permian-age coal. This manuscript was improved with the constructive comments of Carlos Jaramillo, Aaron Diefendorf, and Gordon Inglis.

References

Anagnostou, E., John, E. H., Edgar, K. M., Foster, G. L., Ridgwell, A., Inglis, G. N., et al. (2016). Changing atmospheric CO_2 concentration was the primary driver of early Cenozoic climate. *Nature*, *533*, 380–384. https://doi.org/10.1038/nature17423

Anderson, J. B., Warny, S., Askin, R. A., Wellner, J. S., Bohaty, S. M., Kirshner, A. E., et al. (2011). Progressive Cenozoic cooling and the demise of Antarctica's last refugium. *Proceedings of the National Academy of Sciences of the United States of America*, *108*(28), 11356–11360. https://doi.org/10.1073/pnas.1014885108

Ashworth, A., Lewis, A., Marchant, D., Askin, R., Cantrill, D., Francis, J., et al. (2007). The Neogene biota of the Transantarctic mountains. In A. K. Cooper, C. R. Raymond, et al., (Eds.), *Online Proceedings of the ISAES X, USGS Open-File Report 2007–1047*, p. 4. Extended Abstract 071.

Askin, R. A., Elliot, D. H., Stilwell, J. D., & Zinsmeister, W. J. (1991). Stratigraphy and paleontology of Campanian and Eocene sediments, Cockburn Island, Antarctic Peninsula. *Journal of South American Earth Sciences*, *4*(1), 99–117. https://doi.org/10.1016/0895-9811(91)90021-C

Bakkelund, A., Porter, T. J., Froese, D. G., & Feakins, S. J. (2018). Net fractionation of hydrogen isotopes in *n*-alkanoic acids from soils in the northern boreal forest. *Organic Geochemistry*, *125*, 1–13. https://doi.org/10.1016/j.orggeochem.2018.08.005

Barron, J., Larsen, B., Baldauf, J. G. (Eds.), (1991). Proceedings of the ocean drilling program, 119 scientific results. Ocean Drilling Program. https://doi.org/10.2973/odp.proc.sr.119.1991

Bohaty, S. M., & Zachos, J. C. (2003). Significant Southern Ocean warming event in the late middle Eocene. *Geology*, *31*(11), 1017–1020. https://doi.org/10.1130/G19800.1

Bohaty, S. M., Zachos, J. C., & Delaney, M. L. (2012). Foraminiferal Mg/Ca evidence for Southern Ocean cooling across the Eocene-Oligocene transition. *Earth and Planetary Science Letters*, *317–318*(318), 251–261. https://doi.org/10.1016/j.epsl.2011.11.037

Bohaty, S. M., Zachos, J. C., Florindo, F., & Delaney, M. L. (2009). Coupled greenhouse warming and deep-sea acidification in the middle Eocene. *Paleoceanography*, *24*(2). https://doi.org/10.1029/2008PA001676

Brown, C. A., Riding, J. B., & Warny, S. (2008). *Palynological techniques*. American Association of Stratigraphic Palynologists Foundation, AASP Special Publications.

Cerda-Peña, C., Contreras, S., & Rau, J. R. (2020). Molecular *n*-alkyl leaf waxes of three dominant plants from the temperate forest in South America. *Organic Geochemistry*, *149*, 104105. https://doi.org/10.1016/j.orggeochem.2020.104105

Chen, X., Liu, X., Wei, Y., & Huang, Y. (2019). Production of long-chain n-alkyl lipids by heterotrophic microbes: New evidence from Antarctic lakes. *Organic Geochemistry*, *138*, 103909. https://doi.org/10.1016/j.orggeochem.2019.103909

Colwyn, D. A., & Hren, M. T. (2019). An abrupt decrease in Southern Hemisphere terrestrial temperature during the Eocene-Oligocene transition. *Earth and Planetary Science Letters*, *512*, 227–235. https://doi.org/10.1016/j.epsl.2019.01.052

Coxall, H. K., & Pearson, P. N. (2007). The Eocene-Oligocene transition. In M. Williams, A. M. Haywood, F. J. Gregory, & D. N. Schmidt, (Eds.), *Deep time perspectives on climate change: Marrying the signal from computer models and biological proxies* (pp. 351–387). Geological Society of London. https://doi.org/10.1144/TMS002.16

Coxall, H. K., Wilson, P. A., Pälike, H., Lear, C. H., & Backman, J. (2005). Rapid stepwise onset of Antarctic glaciation and deeper calcite compensation in the Pacific Ocean. *Nature*, *433*(7021), 53–57. https://doi.org/10.1038/nature03135

Cramer, B. S., Toggweiler, J. R., Wright, J. D., Katz, M. E., & Miller, K. G. (2009). Ocean overturning since the Late Cretaceous: Inferences from a new benthic foraminiferal isotope compilation. *Paleoceanography*, *24*(4). https://doi.org/10.1029/2008PA001683

Dearing Crampton-Flood, E., Tierney, J. E., Peterse, F., Kirkels, F. M. S. A., & Sinninghe Damsté, J. S. (2020). BayMBT: A Bayesian calibration model for branched glycerol dialkyl glycerol tetraethers in soils and peats. *Geochimica et Cosmochimica Acta*, *268*, 142–159. https://doi.org/10.1016/j.gca.2019.09.043

DeConto, R. M., Pollard, D., Wilson, P. A., Pälike, H., Lear, C. H., & Pagani, M. (2008). Thresholds for Cenozoic bipolar glaciation. *Nature*, *455*(7213), 652–656. https://doi.org/10.1038/nature07337

De Jonge, C., Hopmans, E. C., Zell, C. I., Kim, J.-H., Schouten, S., & Sinninghe Damsté, J. S. (2014). Occurrence and abundance of 6-methyl branched glycerol dialkyl glycerol tetraethers in soils: Implications for palaeoclimate reconstruction. *Geochimica et Cosmochimica Acta*, *141*, 97–112. https://doi.org/10.1016/j.gca.2014.06.013

Delmotte, M. (1997). *Enregistrements climatiques à Law Dome: Variabilité pour les périodes récentes et pour la déglaciation* (PhD Thesis). Université Joseph-Fourier - Grenoble I. Français. Retrieved from https://tel.archives-ouvertes.fr/tel-00759854/

Diefendorf, A. F., Leslie, A. B., & Wing, S. L. (2015). Leaf wax composition and carbon isotopes vary among major conifer groups. *Geochimica et Cosmochimica Acta*, *170*, 145–156. https://doi.org/10.1016/j.gca.2015.08.018

Douglas, P. M. J., Affek, H. P., Ivany, L. C., Houben, A. J. P., Sijp, W. P., Sluijs, A., et al. (2014). Pronounced zonal heterogeneity in Eocene southern high-latitude sea surface temperatures. *Proceedings of the National Academy of Sciences of the United States of America*, *111*(18), 6582–6587. https://doi.org/10.1073/pnas.1321441111

Duncan, B., McKay, R., Bendle, J., Naish, T., Inglis, G. N., Moossen, H., et al. (2019). Lipid biomarker distributions in Oligocene and Miocene sediments from the Ross Sea region, Antarctica: Implications for use of biomarker proxies in glacially-influenced settings. *Palaeogeography, Palaeoclimatology, Palaeoecology*, *516*, 71–89. https://doi.org/10.1016/j.palaeo.2018.11.028

Ebisuzaki, W. (1997). A method to estimate the statistical significance of a correlation when the data are serially correlated. *Journal of Climate*, *10*(9), 2147–2153. https://doi.org/10.1175/1520-0442(1997)010<2147:AMTETS>2.0.CO;2

Erohina, T., Cooper, A., Handwerger, D., & Dunbar, R. (2004). Seismic stratigraphic correlations between ODP Sites 742 and 1166: Implications for depositional paleoenvironments in Prydz Bay, Antarctica. *Proceedings of the Ocean Drilling Program: Scientific Results*, *188*, 1–21. https://doi.org/10.2973/odp.proc.sr.188.2004

Feakins, S. J., Warny, S., & DeConto, R. M. (2014). Snapshot of cooling and drying before onset of Antarctic Glaciation. *Earth and Planetary Science Letters*, *404*, 154–166. https://doi.org/10.1016/j.epsl.2014.07.032

Feakins, S. J., Warny, S., & Lee, J. E. (2012). Hydrologic cycling over Antarctica during the middle Miocene warming. *Nature Geosciences*, *5*(8), 557–560. https://doi.org/10.1038/NGEO1498

Fietz, S., Martínez-Garcia, A., Rueda, G., Peck, V. L., Huguet, C., Escala, M., & Rosell-Melé, A. (2011). Crenarchaea and phytoplankton coupling in sedimentary archives: Common trigger or metabolic dependence?. *Limnology & Oceanography*, *56*(5), 1907–1916. https://doi.org/10.4319/lo.2011.56.5.1907

Forsberg, C. F., Florindo, F., Grützner, J., Venuti, A., & Solheim, A. (2008). Sedimentation and aspects of glacial dynamics from physical properties, mineralogy and magnetic properties at ODP Sites 1166 and 1167, Prydz Bay, Antarctica. *Palaeogeography, Palaeoclimatology, Palaeoecology*, *260*(1–2), 184–201. https://doi.org/10.1016/j.palaeo.2007.08.022

Freymond, C. V., Kündig, N., Stark, C., Peterse, F., Buggle, B., Lupker, M., et al. (2018). Evolution of biomolecular loadings along a major river system. *Geochimica et Cosmochimica Acta*, *223*, 389–404. https://doi.org/10.1016/j.gca.2017.12.010

Galeotti, S., DeConto, R., Naish, T., Stocchi, P., Florindo, F., Pagani, M., et al. (2016). Antarctic Ice Sheet variability across the Eocene-Oligocene boundary climate transition. *Science*, *352*(6281), 76–80. https://doi.org/10.1126/science.aab0669

Galy, V., Eglinton, T., France-Lanord, C., & Sylva, S. (2011). The provenance of vegetation and environmental signatures encoded in vascular plant biomarkers carried by the Ganges-Brahmaputra rivers. *Earth and Planetary Science Letters*, *304*(1), 1–12. https://doi.org/10.1016/j.epsl.2011.02.003

Goldner, A., Herold, N., & Huber, M. (2014). Antarctic glaciation caused ocean circulation changes at the Eocene-Oligocene transition. *Nature*, *511*(7511), 574–577. https://doi.org/10.1038/nature13597

Gradstein, F. M., & Ogg, J. G. (2012). The chronostratigraphic scale. In *The Geologic Time Scale*, F. M. Gradstein, J. G. Ogg, M. D. Schmitz and G. M. Ogg, (Eds.), Boston:Elsevier, pp. 31–42.

Griener, K. W., Nelson, D. M., & Warny, S. (2013). Declining moisture availability on the Antarctic Peninsula during the Late Eocene. *Palaeogeography, Palaeoclimatology, Palaeoecology*, *383–384*, 72–78. http://doi.org/10.1016/j.palaeo.2013.05.004

Griener, K. W., Warny, S., Askin, R., & Acton, G. (2015). Early to middle Miocene vegetation history of Antarctica supports eccentricity-paced warming intervals during the Antarctic icehouse phase. *Global and Planetary Change*, *127*, 67–78. https://doi.org/10.1016/j.gloplacha.2015.01.006

Harrowfield, M., Holdgate, G. R., Wilson, C. J. L., & McLoughlin, S. (2005). Tectonic significance of the Lambert Graben, East Antarctica: Reconstructing the Gondwanan rift. *Geology*, *33*(3), 197–200. https://doi.org/10.1130/G21081.1

Hill, D. J., Haywood, A. M., Valdes, P. J., Francis, J. E., Lunt, D. J., Wade, B. S., & Bowman, V. C. (2013). Paleogeographic controls on the onset of the Antarctic circumpolar current. *Geophysical Research Letters*, *40*(19), 5199–5204. https://doi.org/10.1002/grl.50941

Hochmuth, K., Gohl, K., Leitchenkov, G., Sauermilch, I., Whittaker, J., Uenzelmann-Neben, G., et al. (2020). The evolving paleobathymetry of the circum-Antarctic Southern Ocean since 34 Ma – A key to understanding past cryosphere-ocean developments. *Geochemistry, Geophysics, Geosystems*. *21*(8), e2020GC009122. https://doi.org/10.1029/2020GC009122

Hochmuth, K., Paxman, G. J. G., Gohl, K., Jamieson, S. S. R., Leitchenkov, G. L., Bentley, M. J., et al. (2020). *Combined palaeotopography and palaeobathymetry of the Antarctic continent and the Southern Ocean since 34 Ma*. PANGAEA. https://doi.org/10.1594/PANGAEA.923109

Hopmans, E. C., Schouten, S., & Sinninghe Damsté, J. S. (2016). The effect of improved chromatography on GDGT-based palaeoproxies. *Organic Geochemistry*, *93*, 1–6. https://doi.org/10.1016/j.orggeochem.2015.12.006

Hopmans, E. C., Weijers, J. W. H., Schefuß, E., Herfort, L., Sinninghe Damsté, J. S., & Schouten, S. (2004). A novel proxy for terrestrial organic matter in sediments based on branched and isoprenoid tetraether lipids. *Earth and Planetary Science Letters*, *224*(1), 107–116. https://doi.org/10.1016/j.epsl.2004.05.012

Houben, A. J. P., Bijl, P. K., Pross, J., Bohaty, S. M., Passchier, S., Stickley, C. E., et al. (2013). Reorganization of Southern Ocean plankton ecosystem at the onset of Antarctic glaciation. *Science*, *340*(6130), 341–344. https://doi.org/10.1126/science.1223646

Houben, A. J. P., Bijl, P. K., Sluijs, A., Schouten, S., & Brinkhuis, H. (2019). Late Eocene Southern Ocean cooling and invigoration of circulation preconditioned Antarctica for full-scale Glaciation. *Geochemistry, Geophysics, Geosystems*. *25*(5), 2214–2234. https://doi.org/10.1029/2019GC008182

Huguet, C., Hopmans, E. C., Febo-Ayala, W., Thompson, D. H., Sinninghe Damsté, J. S., & Schouten, S. (2006). An improved method to determine the absolute abundance of glycerol dibiphytanyl glycerol tetraether lipids. *Organic Geochemistry*, *37*(9), 1036–1041. https://doi.org/10.1016/j.orggeochem.2006.05.008

Hutchinson, D. K., Coxall, H. K., Lunt, D. J., Steinthorsdottir, M., de Boer, A. M., Baatsen, M., et al. (2021). The Eocene-Oligocene transition: A review of marine and terrestrial proxy data, models and model-data comparisons. *Climate of the Past*, *17*(1), 269–315. https://doi.org/10.5194/cp-17-269-2021

Inglis, G. N., Carmichael, M. J., Farnsworth, A., Lunt, D. J., & Pancost, R. D. (2020). A long-term, high-latitude record of Eocene hydrological change in the Greenland region. *Palaeogeography, Palaeoclimatology, Palaeoecology*, *537*, 109378. https://doi.org/10.1016/j.palaeo.2019.109378

Inglis, G. N., Farnsworth, A., Lunt, D., Foster, G. L., Hollis, C. J., Pagani, M., et al. (2015). Descent toward the Icehouse: Eocene sea surface cooling inferred from GDGT distributions. *Paleoceanography*, *30*(7), 1000–1020. https://doi.org/10.1002/2014PA002723

Inglis, G. N., Naafs, B. D. A., Zheng, Y., McClymont, E. L., Evershed, R. P., & Pancost, R. D. (2018). Distributions of geohopanoids in peat: Implications for the use of hopanoid-based proxies in natural archives. *Geochimica et Cosmochimica Acta*, *224*, 249–261. https://doi.org/10.1016/j.gca.2017.12.029

Ivany, L. C., Brey, T., Huber, M., Buick, D. P., & Schöne, B. R. (2011). El Niño in the Eocene greenhouse recorded by fossil bivalves and wood from Antarctica. *Geophysical Research Letters*, *38*(16). https://doi.org/10.1029/2011GL048635

Kennett, J. P. (1977). Cenozoic evolution of Antarctic glaciation, the circum-Antarctic Ocean, and their impact on global paleoceanography. *Journal of Geophysical Research*, *82*(27), 3843–3860. https://doi.org/10.1029/JC082i027p03843

Kvenvolden, K., Hostettler, D., Rapp, F. B. J., & Frank, T. (1991). Aliphatic hydrocarbons in sediments from Prydz Bay, Antarctica. *Proceedings of Ocean Drilling Program: Part B*, *119*, 417–423.

Lear, C. H., Bailey, T. R., Pearson, P. N., Coxall, H. K., & Rosenthal, Y. (2008). Cooling and ice growth across the Eocene-Oligocene transition. *Geology*, *36*(3), 251–254. https://doi.org/10.1130/G24584A.1

Liu, Z., Pagani, M., Zinniker, D., DeConto, R., Huber, M., Brinkhuis, H., et al. (2009). Global cooling during the Eocene-Oligocene climate transition. *Science*, *323*(5918), 1187–1190. https://doi.org/10.1126/science.1166368

Macphail, M. K., & Truswell, E. M. (2004). Palynology of Neogene slope and rise deposits from ODP Sites 1165 and 1167, East Antarctica. *Proceedings of the Ocean Drilling Program: Scientific Results*, *188*, 1–20.

Masson-Delmotte, V., Hou, S., Ekaykin, A., Jouzel, J., Aristarain, A., Bernardo, R. T., et al. (2008). A review of Antarctic surface snow isotopic composition: Observations, atmospheric circulation, and isotopic Modeling. *Journal of Climate*, *21*(13), 3359–3387. https://doi.org/10.1175/2007JCLI2139.1

McKelvey, B. C., Hambrey, M. J., Harwood, D. M., Mabin, M. C. G., Webb, P.-N., & Whitehead, J. M. (2001). The Pagodroma Group – A Cenozoic record of the East Antarctic ice sheet in the northern Prince Charles Mountains. *Antarctic Science*, *13*(4), 455–468. https://doi.org/10.1017/S095410200100061X

McLoughlin, S., Lindström, S., & Drinnan, A. N. (1997). Gondwanan floristic and sedimentological trends during the Permian-Triassic transition: New evidence from the Amery Group, northern Prince Charles Mountains, East Antarctica. *Antarctic Science*, *9*(3), 281–298. https://doi.org/10.1017/s0954102097000370

Meire, L., Mortensen, J., Meire, P., Juul-Pedersen, T., Sejr, M. K., Rysgaard, S., et al. (2017). Marine-terminating glaciers sustain high productivity in Greenland fjords. *Global Change Biology*, *23*(12), 5344–5357. https://doi.org/10.1111/gcb.13801

Motoyama, J. M., Axford, Y., Masterson, A. L., & Osburn, M. R. (2019). Calibration of modern sedimentary δ2H plant wax-water relationships in Greenland lakes. *Quaternary Science Reviews*, *225*, 105978. https://doi.org/10.1016/j.quascirev.2019.105978

O'Brien, P. E., Cooper, A. K., & Richter, C. (2001). *Leg 188 summary: Prydz Bay-Cooperation Sea, Antarctica. Proceedings of the Ocean Drilling Program*. Initial Reports. pp. 1–65.

Pagani, M., Huber, M., Liu, Z., Bohaty, S. M., Henderiks, J., Sijp, W., et al. (2011). The role of carbon dioxide during the onset of Antarctic glaciation. *Science*, *334*(6060), 1261–1264. https://doi.org/10.1126/science.1203909

Passchier, S., Bohaty, S. M., Jiménez-Espejo, F., Pross, J., Röhl, U., van de Flierdt, T., et al. (2013). Early Eocene to middle Miocene cooling and aridification of East Antarctica. *Geochemistry, Geophysics, Geosystems*, *14*(5), 1399–1410. https://doi.org/10.1002/ggge.20106

Passchier, S., Ciarletta, D. J., Miriagos, T. E., Bijl, P. K., & Bohaty, S. M. (2017). An Antarctic stratigraphic record of stepwise ice growth through the Eocene-Oligocene transition. *The Geological Society of America Bulletin*, *129*(3–4), 318–330. https://doi.org/10.1130/B31482.1

Paxman, G. J. G., Jamieson, S. S. R., Hochmuth, K., Gohl, K., Bentley, M. J., Leitchenkov, G., & Ferraccioli, F. (2019). Reconstructions of Antarctic topography since the Eocene-Oligocene boundary. *Palaeogeography, Palaeoclimatology, Palaeoecology*, *535*, 109346. https://doi.org/10.1016/j.palaeo.2019.109346

Pearson, P. N., Foster, G. L., & Wade, B. S. (2009). Atmospheric carbon dioxide through the Eocene-Oligocene climate transition. *Nature*, *461*(7267), 1110–1113. https://doi.org/10.1038/nature08447

Petersen, S. V., & Schrag, D. P. (2015). Antarctic ice growth before and after the Eocene-Oligocene transition: New estimates from clumped isotope paleothermometry. *Paleoceanography*, *30*(10), 1305–1317. https://doi.org/10.1002/2014PA002769

Rose, K. C., Ferraccioli, F., Jamieson, S. S. R., Bell, R. E., Corr, H., Creyts, T. T., et al. (2013). Early East Antarctic Ice Sheet growth recorded in the landscape of the Gamburtsev Subglacial Mountains. *Earth and Planetary Science Letters*, *375*, 1–12. https://doi.org/10.1016/j.epsl.2013.03.053

Scher, H. D., Bohaty, S. M., Smith, B. W., & Munn, G. H. (2014). Isotopic interrogation of a suspected late Eocene glaciation. *Paleoceanography*, *29*(6), 628–644. https://doi.org/10.1002/2014PA002648

Scher, H. D., Bohaty, S. M., Zachos, J. C., & Delaney, M. L. (2011). Two-stepping into the icehouse: East Antarctic weathering during progressive ice-sheet expansion at the Eocene-Oligocene transition. *Geology*, *39*(4), 383–386. https://doi.org/10.1130/G31726.1

Scher, H. D., Whittaker, J. M., Williams, S. E., Latimer, J. C., Kordesch, W. E. C., & Delaney, M. L. (2015). Onset of Antarctic Circumpolar Current 30 million years ago as Tasmanian Gateway aligned with westerlies. *Nature*, *523*(7562), 580–583. https://doi.org/10.1038/nature14598

Schimmelmann, A., Sessions, A. L., & Mastalerz, M. (2006). Hydrogen isotopic (D/H) composition of organic matter during diagenesis and thermal maturation. *Annual Review of Earth and Planetary Sciences*, *34*(1), 501–533. https://doi.org/10.1146/annurev.earth.34.031405.125011

Schouten, S., Huguet, C., Hopmans, E. C., Kienhuis, M. V. M., & Sinninghe Damsté, J. S. (2007). Analytical methodology for TEX86 paleothermometry by high-performance liquid chromatography/atmospheric pressure chemical ionization-mass spectrometry. *Analytical Chemistry*, *79*(7), 2940–2944. https://doi.org/10.1021/ac062339v

Sessions, A. L., Zhang, L., Welander, P. V., Doughty, D., Summons, R. E., & Newman, D. K. (2013). Identification and quantification of polyfunctionalized hopanoids by high temperature gas chromatography-mass spectrometry. *Organic Geochemistry*, *56*, 120–130. https://doi.org/10.1016/j.orggeochem.2012.12.009

Sheldon, N. D., Retallack, G. J., & Tanaka, S. (2002). Geochemical climofunctions from North American soils and application to paleosols across the Eocene-Oligocene boundary in Oregon. *The Journal of Geology*, *110*(6), 687–696. https://doi.org/10.1086/342865

Shepherd, A., Ivins, E., Rignot, E., Smith, B., van den Broeke, M., Velicogna, I., et al. (2018). Mass balance of the Antarctic Ice Sheet from 1992 to 2017. *Nature*, *558*(7709), 219–222. https://doi.org/10.1038/s41586-018-0179-y

Stocchi, P., Escutia, C., Houben, A. J. P., Vermeersen, B. L. A., Bijl, P. K., Brinkhuis, H., et al. (2013). Relative sea-level rise around East Antarctica during Oligocene glaciation. *Nature Geosciences*, *6*(5), 380–384. https://doi.org/10.1038/ngeo1783

Tibbett, E. J., Scher, H. D., Warny, S., Tierney, J. E., Passchier, S., & Feakins, S. J. (2021). *Prydz Bay East Antarctica, biomarker and pollen, 36-33 million years*. NOAA Paleoclimate Database. Retrieved from https://www.ncdc.noaa.gov/paleo/study/32052

Tierney, J. E., & Tingley, M. P. (2014). A Bayesian, spatially-varying calibration model for the TEX_{86} proxy. *Geochimica et Cosmochimica Acta*, *127*, 83–106. https://doi.org/10.1016/j.gca.2013.11.026

Tierney, J. E., & Tingley, M. P. (2015). A TEX_{86} surface sediment database and extended Bayesian calibration. *Scientific Data*, *2*(1), 150029. https://doi.org/10.1038/sdata.2015.29

Tipple, B. J., Meyers, S. R., & Pagani, M. (2010). Carbon isotope ratio of Cenozoic CO_2: A comparative evaluation of available geochemical proxies. *Paleoceanography*, *25*(3). https://doi.org/10.1029/2009PA001851

Tochilin, C. J., Reiners, P. W., Thomson, S. N., Gehrels, G. E., Hemming, S. R., & Pierce, E. L. (2012). Erosional history of the Prydz Bay sector of East Antarctica from detrital apatite and zircon geo- and thermochronology multidating. *Australian Systematic Botany*, *13*(11). https://doi.org/10.1029/2012GC004364

Truswell, E. M., & Macphail, M. K. (2009). Identification of unusual 17β(H)-moret-22(29)-ene in lake sediments. *Australian Systematic Botany*, *22*(2), 57–106. https://doi.org/10.1071/SB08046

Uemura, H., & Ishiwatari, R. (1995). Identification of unusual 17β(H)-moret-22(29)-ene in lake sediments. *Organic Geochemistry*, *23*(7), 675–680. https://doi.org/10.1016/0146-6380(95)00036-E

van de Flierdt, J. J., Hemming, S. R., Goldstein, S. L., Gehrels, G. E., & Cox, S. E. (2008). Gamburtsev Subglacial Mountains provenance of Permian-Triassic sandstones in the Prince Charles Mountains and offshore Prydz Bay: Integrated U-Pb and TDM ages and host-rock affinity from detrital zircons. *Geophysical Research Letters*, *35*(21). https://doi.org/10.1029/2008GL035564

Veevers, J., & Saeed, A. (2008). Gamburtsev Subglacial Mountains provenance of Permian–Triassic sandstones in the Prince Charles Mountains and offshore Prydz Bay: Integrated U–Pb and TDM ages and host-rock affinity from detrital zircons. *Gondwana Research*, *14*(3), 316–342.

Warny, S., Askin, R. A., Hannah, M. J., Mohr, B. A. R., Raine, J. I., Harwood, D. M., et al. (2009). Palynomorphs from a sediment core reveal a sudden remarkably warm Antarctica during the middle Miocene. *Geology*, *37*(10), 955–958. https://doi.org/10.1130/G30139A.1

Warny, S., Kymes, C. M., Askin, R., Krajewski, K. P., & Tatur, A. (2019). Terrestrial and marine floral response to latest Eocene and Oligocene events on the Antarctic Peninsula. *Palynology*, *43*(1), 4–21. https://doi.org/10.1080/01916122.2017.1418444

Warny, S. S., & Askin, R. R. (2011). Vegetation and organic-walled phytoplankton at the end of the Antarctic greenhouse world: Latest Eocene cooling events. In *Tectonic, climatic, and cryospheric evolution of the Antarctic Peninsula* (pp. 193–210). American Geophysical Union. https://doi.org/10.1029/2010SP000965

Wright, N. M., Scher, H. D., Seton, M., Huck, C. E., & Duggan, B. D. (2018). No change in Southern Ocean circulation in the Indian Ocean from the Eocene through Late Oligocene. *Paleoceanography and Paleoclimatology*, *33*(2), 152–167. https://doi.org/10.1002/2017PA003238

Zachos, J. C., Breza, J. R., & Wise, S. W. (1992). Early Oligocene ice-sheet expansion on Antarctica: Stable isotope and sedimentological evidence from Kerguelen Plateau, southern Indian Ocean. *Geology*, *20*(6), 569–673. https://doi.org/10.1126/science.1059412

Zachos, J. C., Pagani, M., Sloan, L., Thomas, E., & Billups, K. (2001). A 40-million-year history of atmospheric CO_2. *Philosophical Transactions of the Royal Society A: Mathematical, Physical and Engineering Sciences*, *292*(5517), 686. https://doi.org/10.1126/science.1059412

Zachos, J. C., Stott, L. D., & Lohmann, K. C. (1994). Evolution of Early Cenozoic marine temperatures. *Geology*, *9*(2), 353–387. https://doi.org/10.1029/93PA03266

Zhang, Y. G., Pagani, M., Liu, Z., Bohaty, S. M., & DeConto, R. (2013). Ring Index: A new strategy to evaluate the integrity of TEX86 paleothermometry. *Philosophical Transactions of the Royal Society A: Mathematical, Physical and Engineering Sciences*, *371*, 20130096. https://doi.org/10.1098/rsta.2013.0096

Zhang, Y. G., Pagani, M., & Wang, Z. (2016). Ring Index: A new strategy to evaluate the integrity of TEX_{86} paleothermometry. *Paleoceanography*, *31*(2), 220–232. https://doi.org/10.1002/2015PA002848